Original Research

Hydrometeorological assessments and suspended sediment delivery from a central Himalayan glacier in the upper Ganga basin

Amit Kumar [a,*], Akshaya Verma [a], Anupam Anand Gokhale [a], Rakesh Bhambri [a], Anshuman Misra [a], Shipika Sundriyal [a], Dwarika Prasad Dobhal [a], Naval Kishore [b]

[a] Centre for Glaciology, Wadia Institute of Himalayan Geology, 33 GMS Road, Dehra Dun, Uttarakhand, India
[b] Centre of Advanced Study in Geology, Department of Geology, Panjab University, Chandigarh, India

ABSTRACT

Integrated hydrometeorological investigations are not frequently available at a regional scale over a longer time period, especially near the terminus of Indian Himalayan glaciers. An integrated approach to the collection of hydrological data has major advantages for understanding the runoff generation mechanisms at basin scale, particularly when coupled with meteorological observations. The current study involves time series analysis of hydrometeorological records collected near the terminus of the Chorabari Glacier, for four consecutive ablation seasons (June–Sept.) 2009–2012. The analysis shows that variation in rainfall was higher ($c_v = 0.9$) at the same elevation over proximal sites, while the intensity of extreme rainfall events was 121–160 mm/d. The diurnal temperature range (DTR) has a tendency to reduce over the ablation season because of the onset of the Indian Summer Monsoon (ISM) and then further increases during the ISM withdrawal indicating humid-temperate conditions. The peak discharge (Q_{peak}) was found to be higher during July and August. Snow and glacier melt contributed 76% of the total suspended sediment transport during peak ISM months (July and August) reflecting seasonal evolution of the hydrologic conduits. The results indicate that Karakoram and western Himalayan glaciers produce comparatively low sediment yield compared to central Himalayan glaciers. The hydrological variations are depicted through flow duration curves (FDC) for meltwater discharge and sediment load. The flow corresponding to Q_{50}, Q_{75}, and Q_{90} (where Q_x is the discharge that is exceeded x percent of the time referred to as % dependability) are 4.2, 3.7, and 2.8 m³/s; and the corresponding dependability for suspended sediment loads (SSLs) are 409.0, 266.0, and 157.2 t/d, respectively. The daily SSL and discharge (Q) from 2009 to 2012 were used to develop a sediment rating curve ($SSL = 39.55 \times Q^{1.588}$, $R^2 = 0.8$). Multiple regressions are used to determine the impacts of meteorological parameters on glacier melt. The meteorological conditions, hydrological characteristics, and suspended sediment delivery for the Chorabari Glacier provide insight on meltwater generation processes and sediment transport patterns during the ISM season.

© 2018 International Research and Training Centre on Erosion and Sedimentation/the World Association for Sedimentation and Erosion Research. Published by Elsevier B.V. All rights reserved.

1. Introduction

The Himalayan Mountain range is the origin of many important glaciers and rivers that composes the largest fresh water reserve outside the Polar Regions, thus, ensuring water supplies to millions of people living downstream. The Indian Himalayan region (IHR) extends between 21°57′ to 37°5′N latitude and 72°40′ to 97°25′E longitude with an area of 0.531 million km², accounting for 16.16% of India's total geographical area (Nandy et al., 2000). In the IHR, the Geological Survey of India has identified 9575 glaciers with an overall area of ~37,500 km² (Sangewar & Shukla, 2009). A long time series of hydrometeorologic data in the Alps, the Caucasus, and the Tien Shan Mountains are available since the early twentieth century (Gao et al., 2013; Li et al., 2010; Li et al., 2016; Sun et al., 2015), but a limited number of Himalayan glaciers have been continuously monitored for developing long term hydrometeorological time series (Haritashyaet al., 2006; Raina, 2009; Srivastava et al., 2014a). In the IHR, various research organizations (e.g., the Geological Survey of India, Centre for Glaciology at Wadia Institute of Himalayan Geology, National Institute of Hydrology, Jawaharlal Nehru University, National Centre for Antarctic and Ocean Research, and various others) have started glaciological
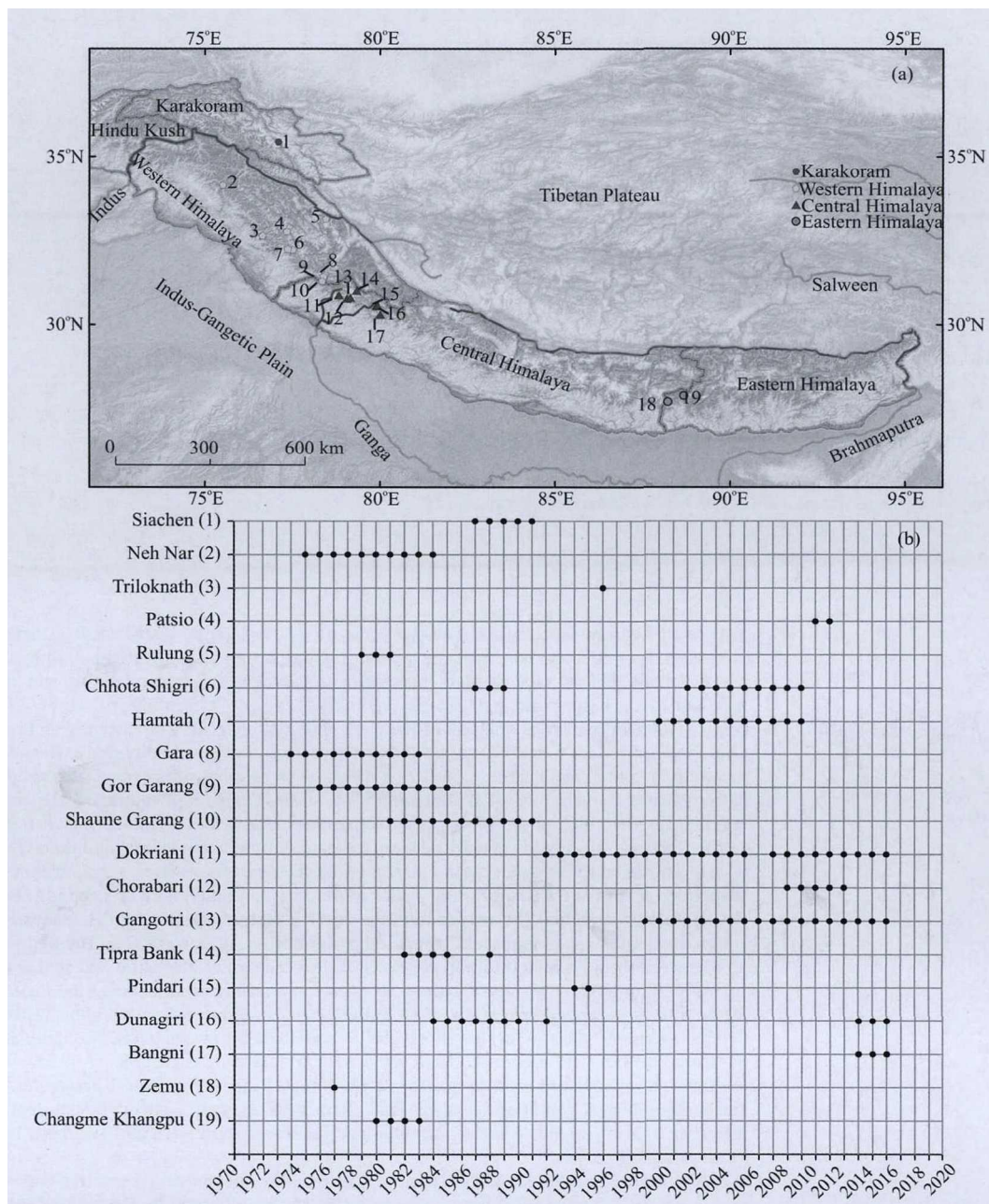
Fig. 1. Locations of glaciers monitored by various research organizations since 1974 in the Indian Himalayan region (a) and availability of hydrological records (discharge measurements) from Karakoram to eastern Himalaya (b).

studies on several Indian Himalayan glaciers, but detailed and continuous hydrometeorological records are not readily available (Fig. 1). A number of studies have conceded the applicability of hydrometeorological records for various glaciological aspects such as mass balance, melt runoff modelling, and particularly for the reconstruction of discharge using linear models and tree ring chronologies (Cánovas et al., 2017; Shah et al., 2013). Other studies on glacier mass balance, glacier hydrology, and glacier fluctuations have provided significant insight on glacier health over the years that are required for future projections under a changing climate (Bhambri et al., 2011; Dobhal et al., 2013; Kumar et al., 2014; Srivastava et al., 2014a, b). Therefore, the long term temperature and precipitation distribution patterns, including other meteorological data, is required for understanding climate change scenarios that are not well recognized over the Himalayan basins (Azam et al., 2016; Bollasina et al., 2002; Suzuki et al., 2007; Tartari et al., 1998).

Meteorological records play a significant role in understanding the spatiotemporal variability, distribution, and magnitude of discharge and sediment yield at higher elevations. Recent occurrences include disasters such as cloudburst leading to rain-induced flash floods and glacial and landslide lake outburst floods paralyzing the daily life of people living in the Himalayan region (Allen et al., 2015; Bhambri et al., 2016; Ruiz-Villanueva et al., 2017). The threshold knowledge of extreme events concurring at higher elevations is still unknown, because of non-availability of hydrometeorological datasets (Allen et al., 2015; Kumar et al., 2017). The scientific community has expressed considerable interest in encompassing hydrometeorological records for managing adverse climatic conditions and weather hazards at higher elevations (Neupane et al., 2014; Ruiz-Villanueva et al., 2017). The knowledge of snowmelt models on meteorological parameters makes a considerable contribution for water resources management and prediction of resultant runoff (Engelhardt et al., 2017;
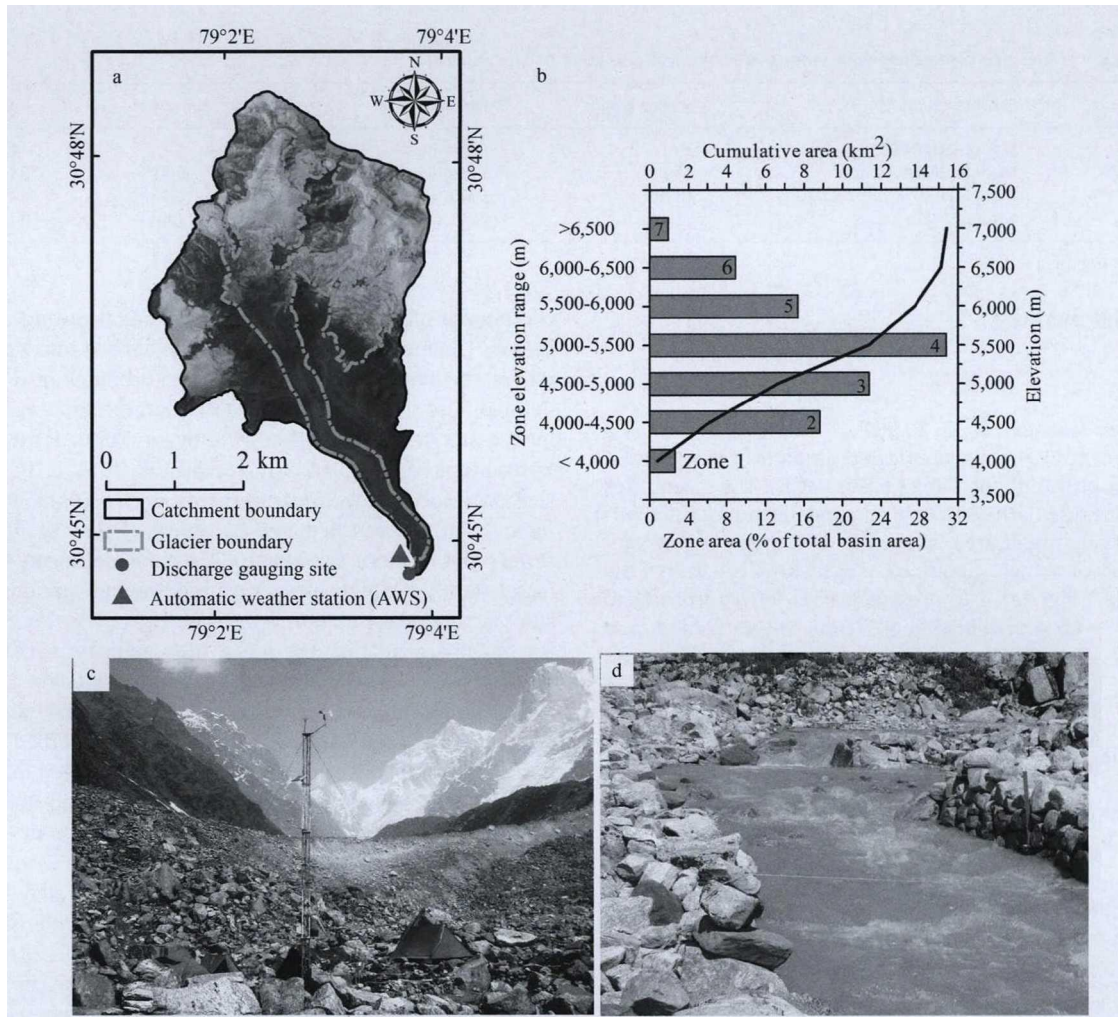
Fig. 2. Landsat imagery showing Chorabari glacierized catchment (a); area–elevation distribution (b); pictorial view of automatic weather station (AWS) installed near the glacier base camp (c); and discharge gauging site near the glacier terminus (d).

Kumar, 2011; Pradhananga et al., 2014; Singh et al., 2010). Therefore, to assess the physical processes governing the melt runoff from glaciers, a better understanding of relations between the prevailing meteorological conditions and glacier mass balance/energy balance is necessary (Andreassen et al., 2008; Azam et al., 2016; Braithwaite, 2009).

Hydrological studies over the Indian Himalayan glaciers have become a necessity as they control the runoff and sediment yield processes in downstream areas and their relative significance for watershed management issues, such as hydroelectric power generation, irrigation, and drinking water supply is paramount (Kumar, 2011). A realistic estimate of suspended sediment transport over the IHR is important as it is associated with snow and glacier melt, especially during the summer season that becomes a challenging problem for running hydropower projects located in high headwater regions of river basins. The debris-covered Himalayan glaciers are the primary source of sediment generation evacuated from subglacial traction zones at very high rates (Arora et al., 2014; Haritashya et al., 2006). This sediment release phenomenon depends upon long/short term storage, diurnal/seasonal variations in discharge characteristics, and meteorological influences upon the glacier (Jansson et al., 2003; Orwin & Smart, 2004; Orwin et al., 2010). Therefore, studies correlating spatiotemporal distribution of melt runoff, sediment sources, and their hydrometeorological control are essential for characterization of

suspended sediment transport dynamics (Haritashya et al., 2010; Kumar et al., 2016; Singh et al., 2003).

The objectives of the current study are to understand the governing hydrometeorological processes at the Chorabari Glacier for four consecutive ablation seasons (2009–2012). The first objective focuses on understanding temporal and seasonal patterns of prevailing weather conditions using in-situ meteorological (Automatic Weather Station) data and its effects on glacier melting processes. The second objective deals with quantitative evaluation of discharge variability and suspended sediment transport patterns to understand hydrological characteristics over the progressive ablation seasons. Detailed information regarding meltwater availability and sediment storage capacity has been estimated through flow and load duration curves. Suspended sediment yield (SSY) has been estimated to understand the erosional processes for the glacierized basin. The relations between meteorological variables, suspended sediment concentration (SSC), and suspended sediment load (SSL) with meltwater discharge have also been established. Similarly, a multivariate statistical technique and time series analysis were used to identify the influence of meteorological variables on meltwater discharge. Furthermore, the meteorological variables, hydrological characteristics, and SSY have been compared with other studies situated in different climatic zones of the Himalayan Mountains.

Table 1
List of meteorological variables monitored along with sensors, accuracy, and resolution of data acquisition.

Observations	Sensors	Sensor height	Resolution	Accuracy	Range
Air temperature	Models HMP45C212	2 m	Daily, hourly	± 0.1°C	−40° to + 60°C
Relative humidity	Models HMP45C212	2 m	Daily, hourly	± 0.8%	0 to 100%
Wind speed	Model 05103 Wind monitor	10 m	Daily, hourly	± 0.3 m/s	0 to 100 m/s
Rainfall	Ordinary rain gauge	Surface	8:30 and 17:30 h; IST[a]	1.0 mm	0 to 4,000 ml

[a] IST represents Indian Standard Time zone

2. Materials and methods

2.1. Study area

The Chorabari Glacier (30°46'20.58"N – 79°02'59.381"E) is a south oriented central Himalayan glacier situated in the Mandakini River basin, of the upper Ganga basin (UGB). The glacier lies upstream of the Kedarnath Shrine, a religious destination for pilgrims. The total catchment area (above the discharge gauging site) is 15.4 km^2 out of which, about 6.6 km^2 (40%) is covered by Chorabari Glacier (Fig. 2a). The present glacier length from head until terminus is ~7.5 km (Dobhal et al., 2013). The catchment and glacier boundary was demarcated using the Landsat imagery and area-elevation distribution curve was prepared from the ASTER (Advanced Spaceborne Thermal Emission and Reflection Radiometer) GDEM (Global Digital Elevation Model).The elevation ranges from ~3800 to ~6500 m above sea level (asl), while the elevation distribution of the glacierized area and its drainage basin is presented in percentage distribution for each elevation zone (Fig. 2b). The major segment of the glacier is concentrated below 5000 m asl in the basin. The elevation distribution of the glaciated area as a percentage of total glacier area shows that maximum glacier area lies between the elevation range of 5000–5500 m asl (31%), followed by 4500–5000 m asl (23%).

2.2. Meteorological data collection

The development of automatic weather stations (AWSs) has significantly reduced the manual errors, temporal delay between meteorological observations, and visualization of measured variables at highly remote sites throughout the year. Automatic weather observations refer to the actions involved in converting signals through sensors, processing and transforming these signals into meteorological data and transmission of the resulting information automatically to the storage device or data logger. In the current study, an AWS (Campbell Scientific) was installed at an elevation of ~3800 m asl on the right bank of the Mandakini River, about 200 m downstream from the glacier terminus (Fig. 2c). The site was selected to obtain observations representing the surrounding area. The AWS is equipped with sensors of air temperature (T), relative humidity (RH), wind speed (WS), and wind direction (WD); details of sensors and frequency of data acquisition are listed in Table 1. Meteorological observations were made continuously during the ablation seasons (2009–2012), using automated sensors, while precipitation in the form of rainfall (R) was observed manually using an ordinary rain gauge (ORG) at the standard frequency in accordance with the guidelines followed by the India Meteorological Department.

2.3. Hydrological data collection

The study area is usually frozen and inaccessible during winter because of extreme weather conditions, therefore, hydrological records were collected throughout the ISM (June-September). Melt runoff generated from the Chorabari Glacier is a derivative component of snow, glacial ice, and rainfall during the ablation season. The meltwater stream was channelized into a gauging site, where the flow was calm and least turbulent in a single well defined flow that represents the discharge estimations calculated by the area–velocity method (Bhutiyani, 2000; Haritashya et al., 2010; Kumar et al., 2014; Srivastava et al., 2014a). The accuracy in surface velocity flow measurements was acceptable, when the mean velocity was calculated by repeating float readings at least three times or more. Ostrem (1964) established a constant velocity factor (0.85) for high elevation mountainous streams. This constant factor and estimated surface velocity of the stream were used for further calculating the mean flow velocity of the meltwater stream. Water levels were recorded manually using a staff gauge, properly cased in a calm spot in the stream (Fig. 2d). Regular cross-sectional measurements are necessary as the riverbed geometry is naturally variable because of high erosion and bed load observed during the ablation season. Therefore, a graduated staff gauge was used for estimation of cross-sectional measurements. Fig. 3 demonstrates a typical relation between stage (H) and discharge (Q) for the Chorabari Glacier developed separately to estimate daily discharge for each ablation season during the study period 2009-2012 (Guerrero et al., 2012; Kumar et al., 2016). A rating curve is obtained from continuous (regular) values of water levels (stage) and discharge throughout the ablation season with an accuracy upto ± 10% (Bhutiyani, 2000; Kumar et al., 2016; Singh et al., 2006).

Suspended sediment samples (n = 964) were collected in clean high density polyethylene (HDPE) bottles (500 ml) at the discharge gauging site twice a day corresponding to the minimum flow at 08:00 and maximum flow at 17:00 for the ablation seasons 2009-2012, (Haritashya et al., 2010; Kumar et al., 2014; Sharp et al., 1995). Samples were collected at the stream mid-depth and filtered at the gauging site using ashless filters. After weighing and oven drying, the SSC for each sample was obtained in mg/l. The SSL is a function of SSC and meltwater discharge, expressed in t/d (Chen et al., 2016; Hallet et al., 1996); whereas, the SSY was computed for the basin above the discharge gauging site throughout the ablation season (June-September). A standard error upto ± 10% was observed in the hydrological datasets in the Siachen Glacier, Karakoram (Bhutiyani, 2000), while other studies for the central Himalayan glaciers found error estimation in quantification of discharge and suspended sediment flux upto ± 5% (Haritashya et al., 2006; Singh et al., 2006; Srivastava et al., 2014a). Furthermore, the collection of hydrometeorological records was discontinued in June 2013 because of the occurrence of an extreme rainfall event known as the Kedarnath disaster (Allen et al., 2015). The statistical characteristics of the hydrometeorological datasets offer basic information about the frequency distribution and time variability of the hydrometeorological data. An elaborate stepwise flow chart of the data collection and analysis applied in this study is shown in Fig. 4.
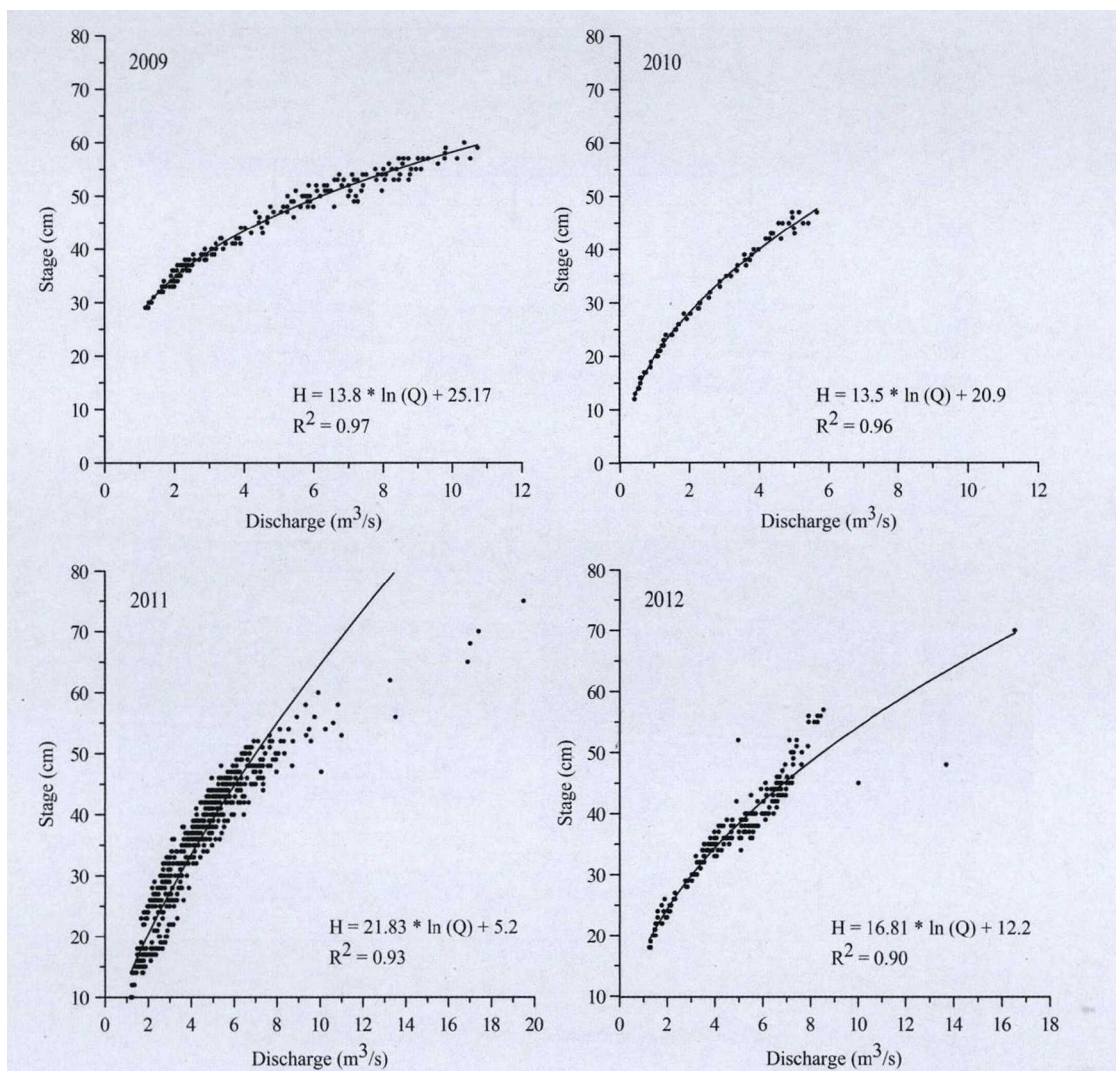
Fig. 3. Relations between stage (H) and discharge (Q) for the Chorabari Glacier meltwater stream for each ablation season, 2009–2012, (Kumar et al., 2016).

3. Results and discussion

3.1. Meteorological observations and analysis

Table 2 summarizes available meteorological records (above 3800 m asl) for the ablation season in central and western Himalayan glaciers. Negligible information is available in eastern part of the IHR and, therefore, to understand spatial variability in meteorological parameters over high elevation stations, published meteorological records from the Pyramid Meteorological Station (PMS) situated in the Khumbu Glacier valley, Nepal Himalaya have been used as representative for eastern Himalayan glaciers (Tartari et al., 1998).

3.1.1. Air temperature

Temperature is an important meteorological variable required for estimation of glacier melting processes such as ablation and generation of melt runoff (Kumar, 2011; Srivastava et al., 2014b). The daily variations in maximum, minimum, and mean temperature for the ablation seasons (2009–2012) can be seen in Fig. 5a. Monthly mean maximum, minimum, and mean temperatures were 12.0, 12.9, 12.4, and 11.2 °C; 4.9, 7.2, 7.5, and 5.0 °C; and 7.8, 9.6, 9.5, and 7.4 °C during the months of June, July, August, and September, respectively. The monthly mean values for maximum, minimum, and mean temperature, illustrate maximum temperature was higher in July followed by August, while minimum

temperature was observed to be higher in August followed by July with a similar pattern observed for the mean temperature. Seasonal variations in mean maximum, minimum, and mean temperature for the ablation seasons (2009–2012) were 12.1, 11.7, 12.3, and 12.4 °C; 5.9, 6.3, 5.6, and 6.4 °C; and 8.4, 8.5, 8.3, and 8.8 °C, respectively. The highest seasonal maximum, minimum, and mean temperature was recorded in the 2012 ablation season. In general, the temperature starts increasing from June to August and further decreases towards the end of the ablation season. As the ablation season advances, a small increase in the maximum air temperature was observed; whereas, significant variability was observed in minimum air temperature owing to seasonal weather fluctuations and existing microclimatic conditions within the basin.

The variability in the prevailing weather conditions over the Chorabari Glacier can be understood using statistical analysis, such as the mean and coefficient of variation (c_v) computed utilizing the daily time series for the ablation seasons (2009–2012). Available temperature records show that, the daily minimum temperature has more variability ($c_v = 0.3$), whereas maximum temperature shows less variability ($c_v = 0.1$; Table 3). During the peak ISM months, i.e. July and August, the cloud cover presence obstructs the shortwave solar radiation that effectively heats the surface during day, while at night the longwave radiation emitted is trapped, thus, decreasing the temperature variability. Similarly, the opposite phenomenon is observed during the onset and
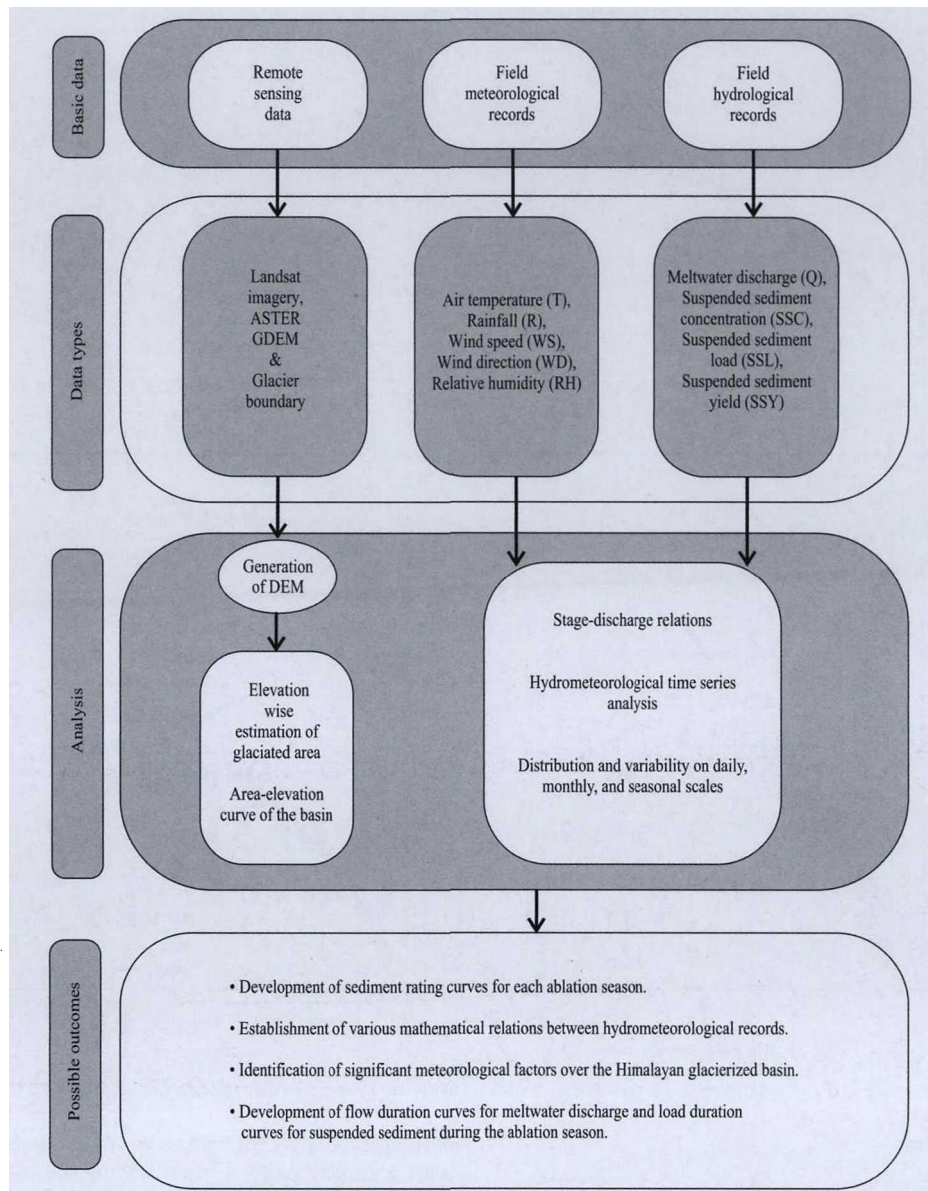
Fig. 4. Graphical representation of methods used in collection and analysis of hydrometeorological data for the Chorabari Glacier. [Note: ASTER (Advanced Spaceborne Thermal Emission and Reflection Radiometer) GDEM (Global Digital Elevation Model) and DEM (Digital Elevation Model)].

Table 2
Summary of high elevation meteorological stations above 3,800 m asl in the Himalayan Mountain range.

Glacier	Basin/ Region	Elevation (m asl)	T_x (°C)	T_n (°C)	T_m (°C)	RH (%)	WS (km/h)	R (mm)	Observation period	Reference
Chorabari	Mandakini/central Himalaya	~3,800	12.1	6.1	8.5	84.0	7.7	1,217.0	(June-Sept., 2009-2012)	Current study
Dokriani	Bhagirathi/central Himalaya	~3,850	12.3	5.7	9.5	88.8	2.3	1,041.0	(June-Sept., 1995-1998)	Singh and Rama-sastri (1999)
		~3,850	13.0	3.8	8.4	–	–	1,370.0	(June.-Sept., 2010-2011)	Kumar et al. (2014)
Gangotri	Bhagirathi/central Himalaya	~3,800	14.7	4.1	9.4	80.0	6.7	259.5	(May-Oct., 2000-2003)	Singh et al. (2005)
Dunagiri	Dhauliganga/central Himalaya	~4,200	14.1	3.6	8.7	86.2	4.6	174.4	(July-Sept., 1984-1989)	Srivastava et al. (2014b)
Chhota Shigri	Chandra/western Himalaya	~4,863	–	–	2.5	68.0	10.0	117.0 [a]	(June-Sept., 2010-2013)	Azam et al. (2016)
Pyramid Meteorological Station (PMS)	Khumbu/eastern Himalaya	~5,035	10.1	-3.4	3.1	91.0	4.5	403.4	(June-Sept., 1994-1996)	Tartari et al. (1998)

T_x = Maximum temperature, T_n = Minimum temperature, T_m = Mean temperature, RH = Relative humidity, WS = Wind speed, R = Rainfall.

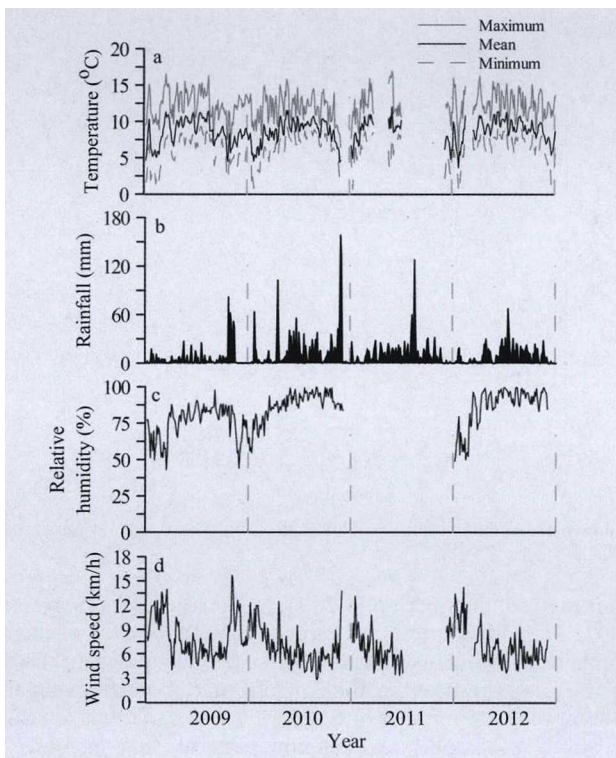[a] R = Seasonal rainfall for the ablation season 2013 at 3,850 m asl.

Fig. 5. Daily distribution of maximum (T_x), minimum (T_n), and mean air temperature (T_m) (a); rainfall (R) (b); relative humidity (RH) (c); and wind speed (WS) (d) for the months of (June–Sept.) during the ablation seasons (2009–2012).

withdrawal of the ISM, which ensures comparatively increasing temperature during the months of June and September.

Insight is also provided on seasonal and monthly diurnal temperature range (DTR = T_x − T_n) for the Chorabari Glacier during the study period (2009–2012, omitting 2011). In the ablation season 2011, the AWS malfunctioned because of the power failure between August and mid-September leading to a data gap in the air temperature measurements. Therefore, the analysis of DTR was not performed for the ablation season 2011. The monthly mean DTR values were 7.5, 5.5, 4.9, and 5.9 °C in the months of June, July, August, and September, respectively. These results suggest that during the onset of ablation in June, the temperature range was the highest because of the presence of seasonal snow cover in the basin. But the DTR decreases during the peak monsoon months, i.e. July and August. The temperature range was lowest during August, indicating the least snow-covered areas, presence of cloud cover, and heavy precipitation resulting in minimum sunshine hours. Similar results were observed for the

Gangotri Glacier where the DTR was highest during onset of ablation and lowest during peak monsoon months (Singh et al., 2007). The mean seasonal DTR observed was 6.4, 5.4, and 5.9 °C for the ablation seasons of 2009, 2010, and 2012, respectively. The maximum DTR was observed for the ablation season of 2009, when the observed total rainfall and average relative humidity were lowest (R = 734.0 mm; RH = 76%); while the minimum DTR was observed for the ablation season of 2010, when the observed total rainfall and average relative humidity were highest (R = 1671.0 mm; RH = 88%). This reflects that precipitation (rainfall) and cloud cover conditions over the Chorabari Glacier resulted in significant variations in seasonal DTR indicating humid-temperate conditions during the ISM season. The mean DTR over the whole study period (2009–2012, omitting 2011) was 5.9 °C, with the mean total rainfall of 1173.4 mm and mean relative humidity of 83.7%.Thus, the DTR analysis confirms that the glaciers receiving higher rainfall amount reflect humid-temperate conditions, while the glaciers receiving lower rainfall amount reflect semi-arid conditions during the ablation season in the UGB (Table 2).

Finally, the recorded temperature for the Chorabari Glacier has been compared with other glacierized basins located in different climatic zones in the Himalayan range (Table 2). Even though these records were collected from different study periods the distribution of central Himalayan glaciers showed similar mean temperatures ranging from 8.4 to 9.5 °C; while the seasonal maximum and minimum temperatures ranged between 12.1 and 14.7 °C and 3.6 and 6.1 °C, respectively (Kumar et al., 2014; Singh & Ramasastri, 1999; Singh et al., 2005; Srivastava et al., 2014b). The Chorabari and Dokriani glaciers are situated in the monsoon dominated zones that show a comparatively higher minimum temperature and lower maximum temperature, while the reverse phenomenon is seen for the Gangotri and Dunagiri glaciers lying in the monsoon deficient zones (Table 2). This confirms the orographic effect on temperature distribution that effectively controls temperature range for the glaciers located in the monsoon dominated and monsoon deficient zones. The temperature distribution for the Chhota Shigri Glacier and Pyramid Meteorological Station (PMS) situated in western and eastern Himalaya, respectively, were much lower because of the elevation difference in the recording stations, varying climatic zones, topographic influence, and cloud cover presence (Azam et al., 2016; Tartari et al., 1998).

3.1.2. Rainfall

The daily rainfall recorded during four consecutive ablation seasons (2009–2012) is shown in Fig. 5b. For the entire ablation period 2009–2012, the frequency distribution analysis clearly shows that the class ranges of 0.1–10 and 10.1–20 mm contribute 41.6 and 18.0% of the total rainfall events; whereas, the class

Table 3
Statistical analysis of hydrometeorological datasets collected at Chorabari Glacier during the ablation seasons (2009–2012).

Months	June	July	Aug.	Sept.	June-Sept.	June	July	Aug.	Sept.	June-Sept.	June	July	Aug.	Sept.	June-Sept.
	M	M	M	M	M	σ	σ	σ	σ	σ	C_v	C_v	C_v	C_v	C_v
Q (m³/s)	2.4	5.0	6.3	3.5	4.4	0.8	1.0	0.9	1.0	1.8	0.3	0.2	0.1	0.3	0.4
SSC (mg/l)	955.0	1,494.1	1,498.8	806.8	1,188.7	221.8	470.2	315.8	117.9	432.7	0.2	0.3	0.2	0.1	0.4
SSL (t/d)	250.7	692.9	852.1	259.7	513.8	118.8	298.8	267.5	85.4	334.7	0.5	0.4	0.3	0.3	0.7
T_n(°C)	4.9	7.2	7.5	5.0	6.1	2.1	0.9	0.9	0.9	1.8	0.4	0.1	0.1	0.2	0.3
T_x(°C)	12.0	12.9	12.4	11.2	12.1	1.7	1.3	1.1	1.4	1.4	0.1	0.1	0.1	0.1	0.1
T_m(°C)	7.8	9.6	9.5	7.4	8.5	1.6	0.9	0.8	0.9	1.4	0.2	0.1	0.1	0.1	0.2
RH (%)	70.1	87.4	90.7	86.0	84.0	7.1	4.4	3.2	10.4	9.9	0.1	0.0	0.0	0.1	0.1
WS (km/h)	9.7	6.8	5.8	8.3	7.7	1.6	1.6	0.8	2.0	2.2	0.2	0.2	0.1	0.2	0.3
R (mm)	3.9	11.2	7.5	16.8	9.9	7.6	11.4	6.3	20.5	13.4	1.9	1.0	0.8	1.2	1.4

M = Mean, σ = Standard deviation, C_v = Coefficient of variation, Q = Discharge, SSC = Suspended sediment concentration, SSL = Suspended sediment load, T_n = Minimum temperature, T_x = Maximum temperature, T_m = Mean temperature, RH = Relative humidity, WS = Wind speed, R = Rainfall.
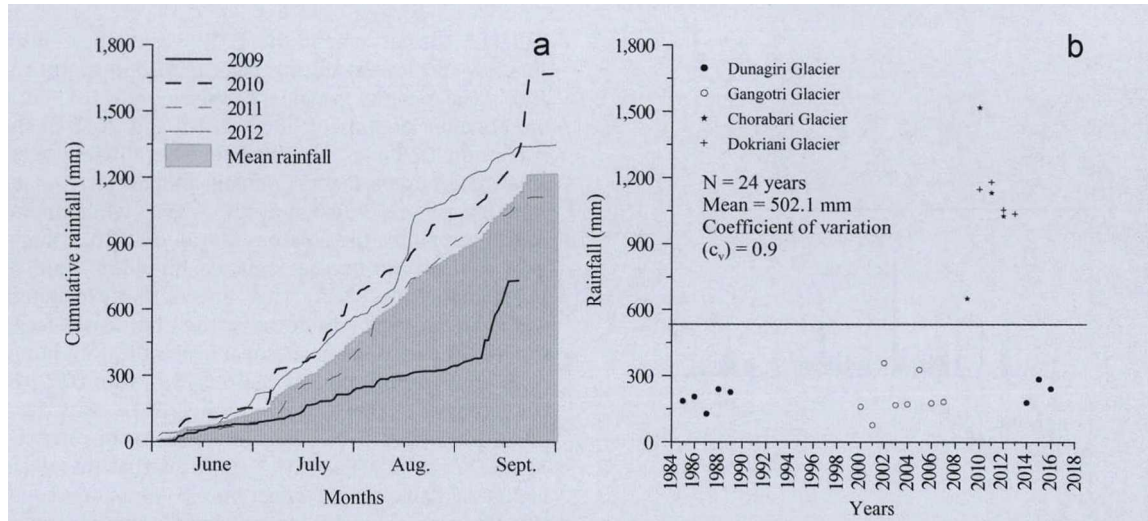
Fig. 6. Cumulative plots of seasonal rainfall (June–Sept.) over the Chorabari Glacier (a), and rainfall distribution (July–Sept.) over the central Himalayan glaciers above an elevation of 3800 m asl (b), during different study periods.

ranges of 20.1–30, 30.1–40, and 40.1–50 mm contribute 7.4, 2.9, and 1.0%, respectively of the total rainfall events. About 3% of extreme rainfall events contributed daily rainfall above the range of > 50.1 mm. These results provide useful information on daily rainfall events and their occurrence that significantly contribute to glacier melt with the advancing ablation season. The monthly mean rainfall distribution of June, July, August, and September was 135.1, 347.6, 397.3, and 337.2 mm, respectively, for the ablation seasons (2009–2012). The valley experiences maximum rainfall in the month of August followed by July, while June received the lowest rainfall. The rainfall in the June is caused by local moisture content causing convective rainfall, while the rainfall during July and August is caused from mixing of local convection and moisture brought by the ISM. The total rainfall for the ablation seasons (2009–2012) was 734.0, 1671.0, 1348.0, and 1115.2 mm, respectively; while the mean total rainfall for the entire ablation period (2009–2012) was 1217.0 mm.

The c_v for rainfall is 1.4, indicating larger variations in daily rainfall over the combined time series for each ablation season. June and September have the highest variability in rainfall (Table 3). The rate at which the rainfall accumulates during any given time interval is called rainfall intensity. The intensity of daily rainfall during the monsoon months has been analyzed by cumulative plots of daily rainfall. High intensity extreme rainfall events are observed during the onset and withdrawal of the ISM in the years 2009 and 2010, indicated by the steep slope of the cumulative plot (Fig. 6a). The seasonal rainfall comparison with three other proximal stations located in the central Himalaya suggests that the rainfall distribution at the same elevation in different basins varies significantly (Kumar, 2011; Kumar et al., 2016; Singh et al., 2003; Srivastava et al., 2014a). These results indicate that the study basin receives the highest rainfall during the ISM season in comparison to other studies at a regional scale (Fig. 6b).

These rainfall analyses indicate the significant influence of the ISM over the central Himalayan region compared to the western Himalayan region. The observed seasonal mean rainfall was compared with other high elevation meteorological stations that ranged between 174.4 and 1370.0 mm (Table 2). The seasonal mean rainfall amount over the Alaknanda and Bhagirathi basins ranged from 174.4 to 1217.0 and 259.5 to 1370.0 mm, respectively; whereas, the mean rainfall over the Chhota Shigri Glacier and PMS ranged between 117.0 and 403.4 mm, respectively. The magnitude of monthly rainfall was maximum in August for all the stations, but the amount varied significantly for other months because of

their regional distribution in different climatic zones (Singh et al., 2007). The Chorabari Glacier receives rainfall for ~74% of the total number of ISM days with the highest frequency during the peak ablation months, whereas, the Gangotri Glacier receives rainfall for ~44% of the total number of ISM days. These variations are caused by strong orographic precipitation patterns that increase at a certain rate with elevation and decreases above a particular elevation (Marquínez et al., 2003). Furthermore, for detailed understanding of the precipitation gradient within a basin, a rainfall intensity-duration threshold should be established if rainfall records (intensity and amount) are available at different elevations (Kumar et al., 2017).

3.1.3. Relative humidity

The data show well observed changes in relative humidity, conceivably with the presence of cloud cover, as well as the distribution of temperature and rainfall during the ablation season. High relative humidity was observed in August, whereas, the lowest humidity was observed in June. The daily distribution of relative humidity during the ablation seasons (2009–2012) is depicted in Fig. 5c. The monthly mean relative humidity observed during ablation, i.e. June, July, August, and September were 70.1%, 87.4%, 90.7%, and 86.0%, respectively. The average relative humidity for the study years 2009, 2010, and 2012 were observed as 76.0% 88.0%, and 87.0%, respectively. The average relative humidity over the study basin is 84.0%. Such distributions imply that, just before the onset and withdrawal of the ISM, air temperature and moisture content is relatively low; while rainfall and cloud cover are less in comparison to the peak ISM months, i.e. July and August. Therefore, the likely combination of such prevailing meteorological conditions would have contributed to the lower relative humidity that can be seen with higher variability (c_v = 0.10–0.12) during June and September compared to July and August (c_v = 0.03–0.05; Table 3). The mean relative humidity over the three climatic zones (i.e. western, central, and eastern Himalayan region) ranged between 68% and 91% (Table 2). Higher moisture content is found over the central Himalayan glaciers having a similar distribution ranging from 80.0% to 88.8%. The lowest RH (68%) was observed at the Chhota Shigri Glacier and the highest with 91% in the eastern Himalayan region. The monthly mean RH was highest at the Chorabari and Dokriani glaciers because of frequent and higher rainy days (Singh & Ramasastri, 1999). These variations in relative humidity are caused by elevational variations in air temperature affecting relative humidity, moisture content, and cloud cover conditions.

Table 4
Summary of available hydrological records above ~3,800 m asl for different climatic zones in the Indian Himalayan region (IHR).

Glacier	Basin/Region	Catchment area (km²)	Mean daily SSC (mg/l)	Mean daily SSL (t/d)	Mean daily Discharge (10⁶ m³)	Observation period	Reference
Chorabari	Mandakini/central Himalaya	15.4	1,188.7	513.8	0.38	(June-Sept, 2009-2012)	Current study
Dokriani	Bhagirathi/central Himalaya	16.1	656.0	446.7	0.86	(June-Sept, 1995-1998)	Singh and Ramasastri (1999)
		15.0	2,324.0	–	0.49	(June-Sept, 2010-2011)	Kumar et al. (2014)
Dunagiri	Dhauliganga/central Himalaya	17.9	229.0	47.0	0.20	(July-Sept, 1984-1989)	Srivastava et al. (2014a)
Tipra Bank	Vishnuganga/central Himalaya	41.6	–	40.0	0.67	(July-Sept, 1981-1988)	Puri and Swaroop (1995)
Gangotri	Bhagirathi/central Himalaya	556.0	1,966.0	16,095.0	5.93	(May-Oct, 2000-2003)	Haritashya et al. (2006); Singh et al. (2006)
			1,310.3	10,392.1	–	(May-Oct, 2008-2011)	Arora et al. (2014)
			1,815.0	11,673.0	5.20	(May-Sept, 2008)	Singh et al. (2014)
Patsio	Chandra-Bhaga/western Himalaya	7.8	38.5	2.8	0.07	(Sept, 2011-2012)	Singh et al. (2015)
Bara Shigri	Chandra/western Himalaya	131.1	886.5	–	–	(July-Sept, 2012-2013)	Singh and Ramanathan (2015)
Chhota Shigri	Chandra/western Himalaya	34.7	370.0	161.0	0.34	(May-Oct, 2010)	Singh et al. (2016)
Batal	Chandra/western Himalaya	–	402.1	–	–	(Aug.-Sept, 2014)	Singh and Ramanathan (2017)
Shaune Garang	Baspa/western Himalaya	33.5	–	30.0	0.41	(July-Sept, 1981-1991)	Raina (2009)
Triloknath	South-Chenab/western Himalaya	–	–	63.0	0.33	(July-Sept, 1995-1996)	Raina (2009)
Hamtah	Chandra/western Himalaya	–	–	127.0	0.38	(July-Sept, 2000-2006)	Raina (2009)
Gara	Baspa/western Himalaya	17.0	–	22.0	0.12	(July-Sept, 1974-1983)	Raina (2009)
Neh Nar	Sind/western Himalaya	8.1	–	6.0	0.10	(July-Sept, 1975-1984)	Raina (2009)
Siachen	Nubra/Karakoram	–	–	8,261.4	8.86	(May-Sept, 1986-1991)	Bhutiyani (2000)
Changme Khangpu	Tista/eastern Himalaya	4.5	–	18.0	0.19	(July-Sept, 1979-1985)	Puri (1999)

3.1.4. Wind regimes

Winds modulate the heat transfer over the mountain slopes affecting moisture content, cloud cover conditions, and glacier melting processes. Daily measurements of surface winds from June to September were taken in order to study the wind velocity, i.e. speed and direction. The daily distribution of wind speed during the ablation season (June–Sept.) for the years (2009–2012) is depicted in Fig. 5d. A maximum seasonal mean wind speed of 15.8 km/h was recorded in the year 2009. Wind velocity shows varying response during the ablation season. Average wind speeds in the months of June, July, August, and September were 9.7, 6.8, 5.8, and 8.3 km/h, respectively, while the average wind speed for the entire ablation period (2009–2012) was 7.7 km/h. The monthly mean wind speed is higher in the months of June and September, while July and September show more variability in wind speed ($c_v = 0.2$) compared to the month of August ($c_v = 0.1$)(Table 3).

During the ablation season, generally wind blows from the south and southwest direction during the day, while the wind direction is reversed during late afternoon or evening. The major reason behind this phenomenon is that during the day the high solar insulation heats up the mountain slopes, heating the air and forcing it upwards; whereas, during the night, the mountain slopes cool down faster than the lower elevations, causing the wind to blow in the opposite direction, i.e. it turns upside down into the valley. The daily mean wind speed ranges from 2.3 to 10.0 km/h for the high elevation meteorological stations (Table 2). These observations indicate that average wind speeds were strongest (10.0 km/h) at the Chhota Shigri Glacier compared to the central Himalayan glaciers that ranged between 2.3 and 7.7 km/h, whereas, the wind speed at PMS was 4.5 km/h.

3.2. Hydrological observations and analysis

Hydrological research at higher elevations, especially in the IHR is lagging because of limited and poor accessibility. Hence, the current hydrological observations deal with the comparison of suspended sediment flux and meltwater discharge with the available records from the Indian Himalayan glaciers during the last four decades (Table 4). Kociuba (2017) measured bedload transport using semi-continuous measurements in two selected cross-sections for a 34 day-long sampling over an Arctic glacier. Rickenmann et al. (2017) monitored the bedload transport at the outlet bypass using a Swiss plate geophone in a hydropower reservoir. Bedload estimation using continuous/direct methods involves measurement by a bedload sampler and numerical equations (Schoklitsch formula) that may lead to errors in the estimation (Warburton, 1990). Such direct and indirect methods cannot be used in the Himalayan meltwater streams as they are highly turbulent with steep gradients that make quantification of bedload transport impossible near the glacier terminus. Therefore, during low flow conditions, the deposited boulders were removed from channelized meltwater stream of the Chorabari Glacier to minimize the errors in quantification of stage-discharge relations. The correlation coefficients for each stage-discharge curve were above $R^2 = 0.90$ which proves the reliability of the discharge data (Fig. 3). The variations in the stage-discharge curves for each ablation season (2009–2012) were caused by seasonal fluctuations in surface ablation, e.g., spatial instabilities influenced by meteorological factors, i.e. air temperature and rainfall events (Collins, 1990; Haritashya et al., 2006; Singh et al., 2006).

3.2.1. Meltwater discharge

Daily discharge for the ablation seasons (2009–2012) is shown in Fig. 7a. The daily distribution of meltwater discharge shows a rising trend from June onwards, reaching its highest in August and descend towards the end of the ablation season. The monthly

mean discharge observed throughout the study period (2009–2012), for June, July, August, and September is 2.4, 5.0, 6.3, and 3.5 m³/s, respectively; while the observed mean discharge for each ablation season (2009–2012) is 4.6, 2.6, 4.5, and 5.7 m³/s, respectively. The mean daily discharge varied from 0.1 to 17.8 m³/s and mean daily discharge for the entire sampling period was observed as 4.4 m³/s.

From 2009–2012, the total discharge magnitude during June and September contributed 14% and 20%, respectively; whereas, the peak monsoon months, i.e. July and August, contributed 66% of the total meltwater discharge. The discharge magnitude at early ablation (June) shows a delayed response because of low temperature, presence of seasonal snow cover and less rainfall events, however, during the mid-ablation (July–August), the temperature rise and frequent rainfall events intensify snow and glacier melting processes. During late ablation (September), the discharge tends to decrease because the release of stored meltwater within the glacier conduits and low air temperature causes frequent refreezing. This discharge pattern confirms the meltwater generation processes within the englacial and subglacial conduits and the water release mechanism is controlled by climatic factors (Jansson et al., 2003; Singh et al., 2006). Analysis of the coefficient of variation (c_v) determines there is variability in discharge during the months of June, July, August, and September because of seasonal changes in different components of the streamflow. The c_v varies from 0.1 to 0.3 during the months of (June–Sept.), while c_v for the entire time series was comparatively higher ($c_v = 0.4$; Table 3).

The mean daily discharge volume draining from Chorabari Glacier has also been estimated and compared with other studies (Table 4). The mean daily discharge volume ranged between 0.07 and 5.93 MCM (million cubic meters) which is highly variable in the Karakoram, western, central, and eastern Himalayan glaciers. This shows significant ISM influence on the discharge volume draining from the central Himalayan glaciers. Table 4 also indicates that the meltwater generation mechanisms are dependent on the glacier size, aspect, basin area, and prevailing microclimatic conditions over the Indian Himalayan glaciers.
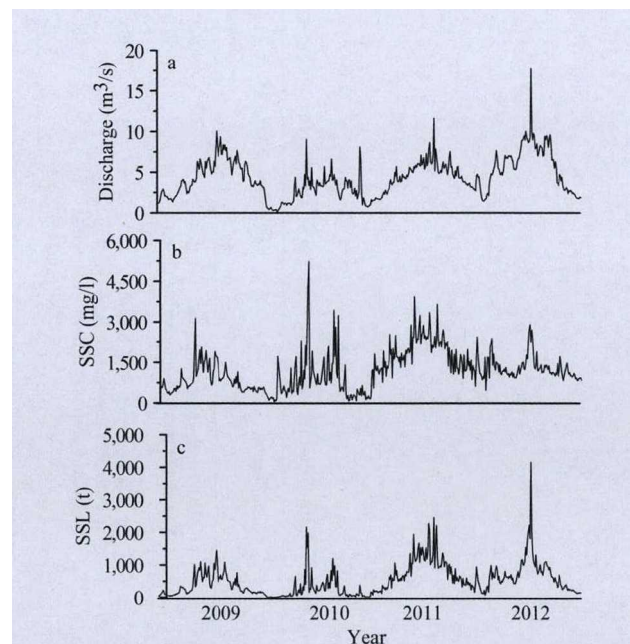

Fig. 7. Daily distribution and variations in meltwater discharge (Q) (a); suspended sediment concentration (SSC) (b); and suspended sediment load (SSL) (c) during the ablation seasons (2009–2012).

3.2.2. Suspended sediment transport patterns

Daily variations in the SSC for the ablation seasons (2009–2012) are shown in Fig. 7b. The SSC in daily discharge was highly and significantly variable over the ablation season showing a rising trend from June onwards, reaching its highest at the end of July and mid-August; and finally declining trend towards the end of the ablation season. The monthly average sediment concentrations for the ablation months (June–Sept.) were 955.0, 1494.1, 1498.8, and 806.8 mg/l, respectively, whereas, the average seasonal concentrations for each ablation season over the study period (2009–2012) were 851.0, 813.9, 1827.2, and 1296.9 mg/l, respectively. Average daily SSC varied between 45.0 and 5232.0 mg/l, while the average SSC over the entire sampling period was 1188.7 mg/l.

The SSC distribution follows the discharge pattern where, June and September contributed 20% and 16% of the total concentrations, whereas, the peak ISM months contributed 64% of the total SSC for all the ablation seasons. SSC variations are basically caused by continuous sediment supply from frictional melting of debris-rich basal ice and melting of moraine-laden ice blocks (Collins, 1990). Similar observations are seen for the Gangotri Glacier where rising and declining of SSC patterns were dependant on fluctuations in air temperature and frequent rainfall events (Haritashya et al., 2006). For understanding the sediment delivery pattern, the estimated SSC has been compared with other Himalayan glaciers located in different climatic zones (Table 4). The mean daily SSC estimated over the IHR ranged from 38.1 to 2324.0 mg/l. The mean daily SSC ranged between 229.0 to 2324.0 and 38.1 to 886.5 mg/l for the central and western Himalayan glaciers, respectively. Negligible records are available from Karakoram and eastern Himalayan glaciers. These results confirm that central Himalayan glaciers produce the highest SSC which is dependent on meteorological conditions over the glacier and the amount of resultant runoff.

Daily variations in the SSL for the ablation seasons (2009–2012) are shown in Fig. 7c. The SSL in the observed daily discharge shows a rising trend from June onwards, reaching its highest in

August and tends to reduce towards the end of the ablation season. The average daily SSL ranged between 1.5 and 4155.0 t/d with the overall average SSL observed for the ablation period (2009–2012) at 513.8 t/d. The monthly average sediment loads for each ablation month (June–Sept.) were 250.7, 692.9, 852.1, and 259.7 t/d, respectively. The total seasonal loads for each ablation season over the study period (2009–2012) were 46.32×10^3, 26.83×10^3, 94.56×10^3, and 82.65×10^3 t, respectively. The mean total suspended sediment load over the study period (2009–2012) was 62.59×10^3 t.

The variability in the SSL is much higher ($c_v = 0.7$) than in SSC ($c_v = 0.4$), the reason being that SSL is dependent on both discharge and SSC (Table 3). From 2009–2012, about 14% of the meltwater discharge was released in June that transported 12% of the total SSL, while the discharge of July and August amounted for 29% and 37% of the total flow volume that transported 34% and 42% of the total SSL. This means that the Chorabari Glacier evacuated 76% of the total sediment load from its internal drainage network during the peak ablation months. The discharge of September amounted for 20% of the total flow volume corresponding to 12% of the total SSL confirming seasonal evolution of the subglacial drainage networks where the sediment flux was drained out towards the end of the ablation season. Haritashya et al. (2006) found similar SSL patterns for the Gangotri Glacier where the high variability was observed because of less sediment availability within the glacier conduits towards the end of ablation season. The estimated SSL shows distinct variations ranging from 2.8 to 16,095.0 t/d over the IHR (Table 4). An overall comparison of the available mean daily SSL record indicates that the magnitude of sediment production and transportation during the ablation seasons is diverse for different climatic regimes. Variations in SSL are found because of different lithologies, varying meteorological conditions, subglacial drainage patterns, and heterogeneity in size and debris cover percentage of the glaciers (Bhutiyani, 2000; Collins, 1989, 1990; Raina, 2009; Singh et al., 2016).

3.2.3. Sediment yield characterization of glacierized basins

Suspended sediment budgets can be used as an indicator for identifying sediment mobilization, and delivery processes and implementing management strategies on a basin scale (Walling & Collins, 2008; Liu et al., 2017). Various difficulties have arisen in fully understanding sediment delivery characteristics, since the quantification is limited only to suspended sediment measurements during the ablation seasons. Therefore, considering such limitations monthly and seasonal suspended sediment yield has been summarized for the Chorabari Glacier in Table 5. The monthly mean SSY's for June ($C_v = 0.9$; Table 5), i.e. during the onset of the

Table 5
Monthly and seasonal suspended sediment yield (SSY) distribution for the Chorabari Glacier during the ablation seasons (2009–2012).

Months	2009	2010	2011	2012	Mean	c_v
June	256.2	45.1	667.2	973.7	485.6	0.9
July	1,069.7	828.0	1,957.8	1,666.8	1,380.6	0.4
August	1,304.9	742.6	2,544.2	2,218.1	1,702.4	0.5
September	377.0	126.4	971.1	508.5	495.8	0.7
Yield (t/yr.km²)	3,007.7	1,742.1	6,140.3	5,367.0	4,064.3	0.5

Table 6
Summary of specific suspended sediment yield (SSY) over different climatic regimes in the Karakoram, Himalayan, and high-Arctic Alpine glaciers.

| Glacier	Basin/Region	Catchment area (km²)	Specific SSY (t/yr.km²)	Observation period	References
Chorabari	Mandakini/central Himalaya	15.4	4,064.3	(June–Sept., 2009-2012)	Kumar et al. (2016)
Dokriani	Bhagirathi/central Himalaya	16.1	2,800.0	(June–Sept., 1995-1998)	Singh et al. (2003)
Dunagiri	Dhauliganga/central Himalaya	17.9	296.3	(July–Sept., 1984-1989)	Srivastava et al. (2014a)
Gangotri	Bhagirathi/central Himalaya	556.0	4,834.0	(May–Oct., 2000-2003)	Haritashya et al. (2006)
			2,863.0	(May–Oct., 2008-2011)	Arora et al. (2014)
			7,663.0	(May–Sept., 2008)	Singh et al. (2014)
Patsio	Chandra-Bhaga/western Himalaya	7.8	132.0	(Sept., 2011-2012)	Singh et al. (2015)
Chhota Shigri	Chandra/ western Himalaya	34.7	1,689.0	(May–Oct., 2010)	Singh et al. (2016)
Siachen	Nubra/Karakoram	–	707.2	(May–Sept., 1986-1991)	Bhutiyani (2000)
Batura	Hunza/Karakoram	650.0	6,086.0	(April–Oct., 1990)	Collins (1996)
Scott Turnerbreen	Central Spitsbergen, Svalbard	12.8	530.0	(1993)	Hodgkins et al. (1997)
Finsterwalderbreen	van Keulenfjorden, Svalbard	68.0	2,250.0	(1999-2000)	Hodgkins et al. (2003)
Haut Glacier d'Arolla	Valais, Switzerland	12.7	4,500.0	(May–Sept., 1989-1990)	Sharp et al. (1995)
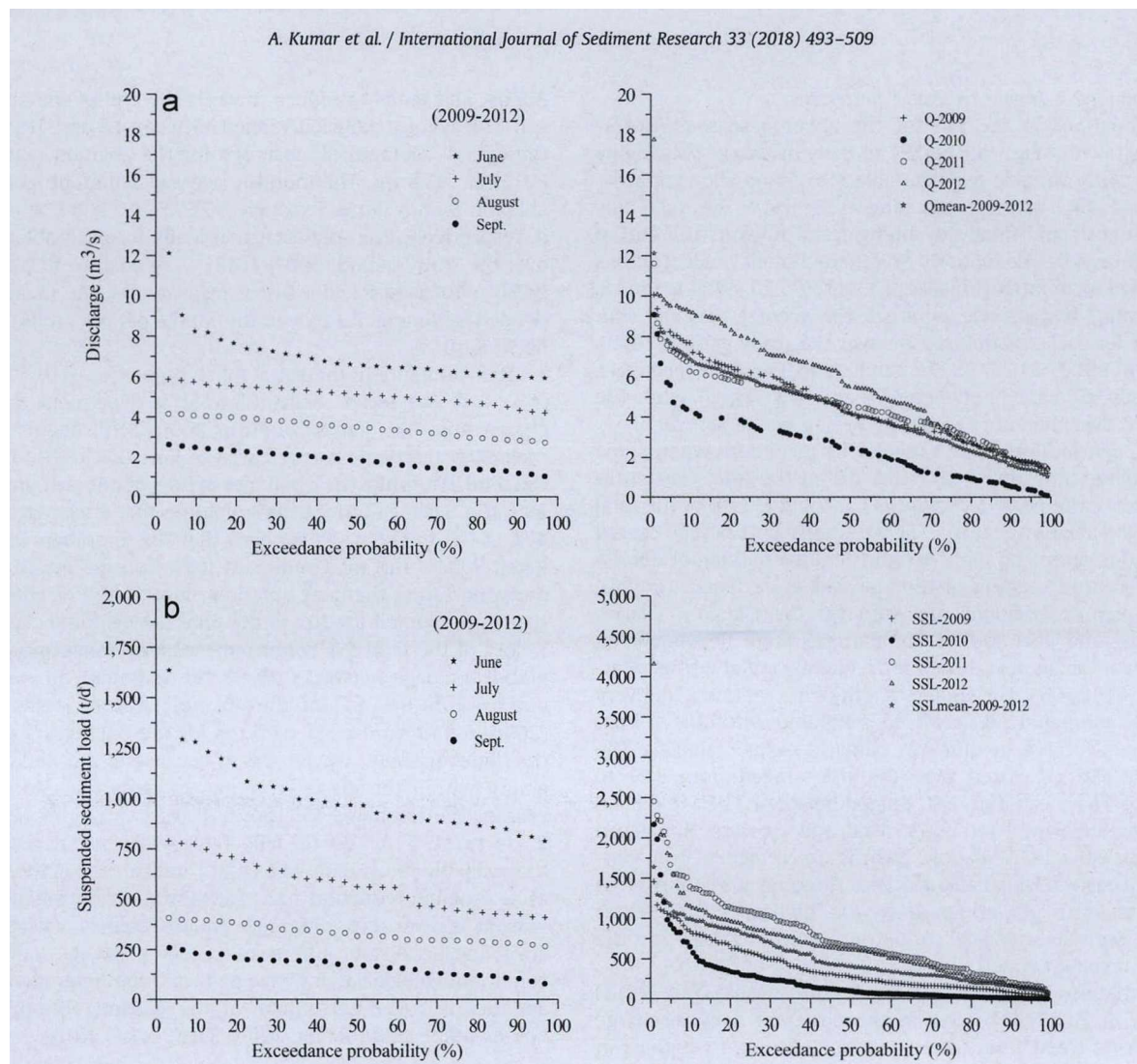
Fig. 8. Monthly mean and seasonal flow duration curves (FDC) for meltwater discharge (a), and mean sediment load duration curves (b), for the Chorabari Glacier during the ablation seasons (2009–2012).

ablation season are usually associated with seasonal snowmelt. In July ($c_v = 0.4$) and August ($c_v = 0.5$), sediment fractions are evacuated from seasonal discharge and higher rainfall caused by the ISM. Finally, during September ($c_v = 0.7$) the SSY declines reflecting sediment depletion with the seasonal evolution of subglacial drainage system. Seasonal SSY for each ablation seasons (2009–2012) were 3007.7, 1742.1, 6149.3, and 5367.0 t/yr.km², respectively. These monthly and seasonal variations in SSY are influenced by the seasonal snow cover, meteorological conditions over the glacier, sediment mobilization processes, and hydrological events in the subglacial conduits (Collins, 1989, 1990). Kumar et al. (2016) estimated the mean SSY ($c_v = 0.5$) at 4064.3 t/yr.km² (Table 5).

The mean specific SSY value is very high compared to the SSY reported from other Indian Himalayan glaciers. These values are compared with the other alpine glaciers and high-Arctic glaciers in Table 6. The estimated SSY for the central Himalayan glaciers is very high and may not correspond to high discharge years (Arora et al., 2014; Haritashya et al., 2006; Singh et al., 2003). The SSY reported for the Karakoram and western Himalayan glaciers are comparatively lower than the central Himalayan glaciers because of different climatic regime, bedrock lithology, and meteorological influence (Bhutiyani 2000; Singh et al., 2015; Singh et al. 2016). Sediment yields in the high-Arctic glaciers (Scott Turnerbreen and Finsterwalderbreen) have a varied range because of thermal regime in the glacier drainage system and the sediment supply

available from the subglacial traction zones (Hodgkins et al., 1997, 2003). Sharp et al. (1995) reported a very high solid denudation rate (SSY) over an alpine glacier (Haut Glacier d'Arolla) that effectively increased the solute denudation rate by > 1.5% compared to the solid denudation rate. These results indicate that significant changes in sediment rates occur in the seasonal distribution caused by instabilities in glacier conduits, hydroclimatic control, delay characteristics of meltwater discharge, thermodynamic behavior of the glacier, and sediment stored within the subglacial waters; thus, highlighting the variability in the glacierized basins (Collins, 1996; Hallet et al., 1996; Singh et al., 2011).

3.2.4. Flow and load duration curves

Frequency analysis using flow duration curves (FDC) demonstrates the availability of meltwater discharge and sediment delivery at different time intervals during the ablation season. The most important variable is to understand the particular time percentage when the rivers exceed a certain value known to deliver high sediment fluxes with the meltwater stream (Arora et al., 2005; Smahtkin, 2001; Vogel & Fennessey, 1994). These duration curves have frequently been used in various hydrological studies, including sediment load transport studies near the glacier terminus (Li et al., 2016). The stream flow data are arranged in a descending order of discharges. If (N) numbers of data points are used, then the plotting position (P) of any discharge (Q) at order m

Table 7
Monthly and seasonal meltwater discharge (m^3/s) and suspended sediment load (t/d), corresponding to Q_{50}, Q_{75}, and Q_{90} and SSL_{50}, SSL_{75}, andSSL_{90} % dependability, respectively,using flow duration curves (FDC).

Flow corresponding to different dependability					
	June	July	Aug.	Sept.	June–Sept.
Q_{50}	6.6	5.1	3.5	1.8	4.2
Q_{75}	6.2	4.7	3.1	1.4	3.7
Q_{90}	6.0	4.3	2.8	1.2	2.8
Sediment load corresponding to different dependability					
SSL_{50}	965.4	561.0	316.0	171.7	409.0
SSL_{75}	879.3	442.8	295.5	124.8	266.0
SSL_{90}	813.5	424.7	282.0	102.9	157.2

is

$$P = (m/N+1) ñ 100$$

Fundamentally, an arithmetic scale, semi–log, or log–log scale is used depending upon the available range of datasets. The flow duration curve simply represents the cumulative frequency distribution indicative of average stream flow and sediment flux variations during the study years. The ordinate, Q_p, for the percentage probability, P_p, represents the flow magnitude that can be expected to be equalled or exceeded P_p % of the time and is termed as P_p% dependable flow. Such flow duration analysis is useful in comparing the flow value of different streams, evaluating a range of dependable flows in water resources project planning (large dam, run-of-the-river projects, and small hydropower schemes), drainage system designs, and flood control studies for river basins.

The flow values corresponding to 50%, 75%, and 90% dependability were estimated as 4.2, 3.7, and 2.8 m^3/s, respectively. For the given study period (2009–2012), the four FDC's constructed will differ because of the variable response of meteorological parameters and other basin characteristics (Arora et al., 2005). The FDC's for monthly mean meltwater discharge were almost flat by month in June through September, but steep curves were found in June (Fig. 8a; Table 7). The flat curves reflect the continuous availability of meltwater discharge indicating the snow and glacier melting processes, storage characteristics, and developed inter-drainage network within the glacier throughout the ablation season; while the steep curves indicate seasonal snow melt at higher rates caused by temperature rise and heavy rainfall events. It is concluded that the daily mean discharge for a specific time period (ablation season) and the corresponding FDC are determined by both meteorological conditions and the hydrological characteristics over the glacier basin.

The duration curves for suspended sediment load corresponding to 50, 75, and 90% dependability were estimated as 409.0, 266.0, and 157.2 t/d, respectively. The load duration curves showed similar results to the flow duration curves, i.e. almost flat throughout the ablation season and steeper in June (Fig. 8b; Table 7). This confirms that seasonal snow cover plays an important role in generating meltwater discharge and sediment delivery patterns for the Indian Himalayan glaciers. However, changes in basin conditions can also contribute to changes in duration curves over time. This integrated study has further room for improvement by using larger datasets, especially in winter or lean periods that are currently unavailable for any Indian Himalayan glacier.

3.3. Time series analysis of hydrological data

Various studies have used time series, regression, and correlation analyses for forecasting discharge from alpine and high-Arctic
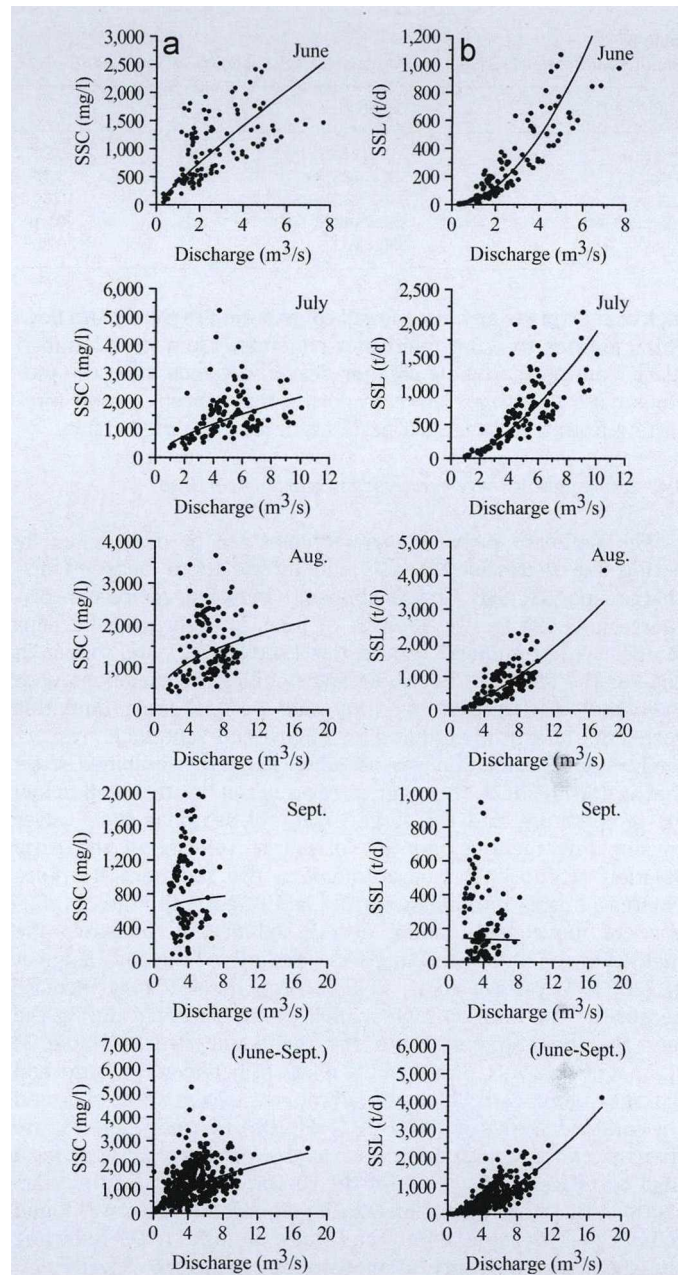

Fig. 9. Monthly and seasonal correlations between discharge (Q) and suspended sediment concentration (SSC) (a), and discharge (Q) and suspended sediment load (SSL) (b), for the Chorabari Glacier during the ablation seasons (2009–2012).

glacierized basins (Shea et al., 2005; Stenborg, 1970; Wolfe & English, 1995). These statistical analyses have also been performed successfully for discharge simulation in the central Himalayan glacierized basins using hydrometeorological records (Singh et al., 2000, 2010; Srivastava et al., 2014b). Li et al. (2016) successfully used statistical analyses using hydrometeorological variables for simulating and predicting discharge over a glacierized basin situated in the southeast Tibetan Plateau. Therefore, daily meltwater discharge autocorrelations for each ablation season have been analyzed. Discharge autocorrelation varied from 0.9 to 0.8 for a time lag of 0 to 2 days during all the ablation seasons and further reduces with increasing time lag. The decline in discharge autocorrelations with time can be explained by the storage characteristics of the subglacial drainage system and the precipitation distribution within the basin. For the given time lags, significant discharge autocorrelations exists for all the ablation seasons. A high degree of discharge autocorrelation indicates strong

Table 8
Monthly and seasonal sediment rating curves for the ablation seasons (2009–2012).

2009-2012	Equations	R^2
June	$SSL=33.48 \times Q^{1.92}$	0.90
July	$SSL=41.88 \times Q^{1.648}$	0.75
August	$SSL=54.79 \times Q^{1.418}$	0.64
September	$SSL=148.62 \times Q^{-0.62}$	0.01
Jun. – Sep.	$SSL=39.55 \times Q^{1.588}$	0.80

Table 9
Correlation matrix for hydrometeorological variables during the ablation seasons 2009–2012 (values are significantly different from zero at the 5% level).

(2009–2012)	Q	SSC	SSL	R	T_n	T_x	T_m	RH	WS	WD
Q	1.0	0.4	0.8	0.2	0.5	0.2	0.4	0.4	-0.3	0.0
SSC		1.0	0.8	0.1	0.4	0.3	0.4	0.3	-0.3	-0.1
SSL			1.0	0.2	0.5	0.3	0.5	0.4	-0.4	0.0
R				1.0	0.0	-0.3	-0.1	0.3	0.0	-0.2
T_n					1.0	0.5	0.9	0.6	-0.6	-0.1
T_x						1.0	0.8	-0.1	0.0	0.2
T_m							1.0	0.4	-0.4	0.0
RH								1.0	-0.8	-0.5
WS									1.0	0.2
WD										1.0

Q = Discharge, T_n = Minimum temperature, T_x = Maximum temperature, T_m = Mean temperature, RH = Relative humidity, WS = Wind speed, WD = Wind direction, R = Rainfall.

meltwater storage and less rainfall contribution to the stream flow. This indicates that the meltwater generated from the Chorabari Glacier during the whole ablation season depends upon the previous day's discharge. Therefore, using this concept, runoff forecasting from the glacierized basin becomes more predictable.

3.4. Interrelations between hydrometeorological data

The sediment delivery characteristics can be determined by performing regression analysis and interrelations between discharge and SSC/SSL. The relationship between meltwater discharge and SSC for the months of June, July, August, and September with combined time series (2009–2012) are shown in Fig. 9a. The SSC does not show any significant correlations with meltwater discharge on monthly and seasonal scales and this correlation drastically reduces for August and September, respectively. A poor correlation was also observed in the combined series during (2009–2012). This poor correlation can be attributed to low air temperature and the large extent of seasonal snow cover causing low melting and low discharge velocity in the early ablation season that cannot mobilize the sediment fractions, whereas, during mid-ablation (July and August) the direct influence of monsoonal rainfall events significantly increases the meltwater generation and suspended sediment transport (Singh et al., 2003; Srivastava et al., 2014a). Also, the SSC may increase because of the unusual high rainfall events observed during the late ablation (September) to the meltwater stream (Table 3) (Kumar et al., 2014). However, the relations between discharge and SSL show good correlations for all months except September and the combined series of (2009–2012; Fig. 9b). Discharge and SSL are directly related to each other since load = discharge x SSC giving a high correlation (R^2 = 0.8) for the combined series for the years (2009–2012). The correlations during monsoon months was found to be higher for some months and varied from 0.4 to 0.9 reflecting the significant influence of meteorological factors, i.e. air temperature and daily rainfall events. The poor correlation observed during late ablation (i.e. September) confirms that the glacier has released its available sediment content with the meltwater. The correlation equations between discharge and SSL, or sediment rating curves, for each month and the whole season are listed in Table 8. Various studies have reported such high correlations for other Indian Himalayan glaciers (Bhutiyani, 2000; Haritashya et al., 2006; Srivastava et al., 2014b).

Correlations between meltwater discharge and air temperature using time series 2009–2012 are listed in Table 9. The analysis reflects that the discharge is correlated with minimum temperature, while there is little or no correlation with the mean and maximum temperature during the ablation seasons (2009–2012). The correlation between discharge and the maximum temperature is R^2 = 0.2 reaching a value of 0.4 for the mean temperature and 0.5 for the minimum temperature. This correlation indicates that by night temperature may play an important role in glacier melting. The incoming solar radiation absorbed by the glacier during the day controls glacier melting during the night in the form of long-wave radiation. By combining series of all the years, results show the importance of minimum temperature for

generating discharge in a glacierized basin. Similarly, the correlation between discharge and relative humidity yields an insignificant R^2 = 0.4, while at the same time relative humidity is correlated poorly with rainfall. Such poor correlations are caused by lower rainfall contribution to meltwater generation by the glacier under low temperature conditions. Such prevailing weather conditions over the glacier indicate snowfall over major parts of the glacier that inhibits the melting process, thus, reducing the discharge. Another important thing to be discussed is that the rainfall amount in the basin is quite low in comparison to the discharge amount draining from the glacier. Wind speed and wind direction are yields poor and insignificant correlation coefficient with meltwater discharge. The significance level for analyses of the correlation matrix is 0.05. Thus, the meltwater generated from the Chorabari Glacier are affected by surface ablation and differential energy conditions because of air temperature causing significant variations in resultant streamflow for each ablation seasons.

3.5. Development of Multivariate Regression Model (MLR)

Stepwise regression is a technique to select multiple variables for the development of multiple regression models that begins by taking into consideration all parameters and subsequently removing insignificant terms stepwise, until only significant terms remain. A hypothesis behind using this method is that some input variables in a multiple regression do not have a significant descriptive outcome on the response. If this explanation is true, then conveniently only the statistically significant terms in the model are kept. The selected variables may be correlated with each other as they are with the response. Considering this explanation, the inclusion of one variable in the model may cover the effect of other input variables.

For daily discharge estimation from the Chorabari Glacier, multiple regression equations were developed separately for each ablation season (2009–2012) along with a regression equation for the combined time series for all the ablation seasons. Multiple linear equations were developed by selecting the climatic variables that may significantly influence the meltwater discharge. The meltwater discharge (Q) was selected as the dependent variable, while variables like T_x, T_n, T_m, R, and WS, were used as independent variables. Multiple regression equations were obtained through stepwise regression and the corresponding correlation values for all the seasons are listed in Table 10. Some of the variables were dropped in the regression equations owing to their statistical insignificance determined by the stepwise regression approach. The R^2 value for the selected ablation seasons varies between 0.6 and 0.7, showing that meltwater discharge is reasonably characterized by these equations. Few other studies have

Table 10

Multivariate regression equations developed for each ablation season and their combined series in different Indian Himalayan and high-Arctic alpine glaciers.

Glacier basin	Latitude-Longitude	Year	Equations	R^2	Reference
Indian Himalayan glaciers					
Chorabari Glacier, Mandakini Basin	30°41′-30°48′N 79°1′-79°6′E	2009	$Q_i = 5.705 + 0.525T_{ni} - 0.291T_{xi} + 0.202T_{mi} + 0.021R_i - 0.005WD_i - 0.535WS_i$	0.6	Current Study
		2010	$Q_i = -1.403 + 0.407T_{ni} - 0.322T_{xi} + 0.501T_{mi} + 0.035R_i - 0.001WD_i - 0.375WS_i$	0.6	
		2011	$Q_i = 2.186 - 0.056T_{ni} - 0.008T_{xi} + 0.269T_{mi} + 0.046R_i + 0.007WD_i - 0.33WS_i$	0.7	
		2012	$Q_i = -1.613 - 0.008T_{ni} - 0.347T_{xi} + 1.393T_{mi} + 0.076R_i - 0.002WD_i - 0.480WS_i$	0.5	
		(2009-2012)	$Q_i = 1.550 + 0.189T_{ni} - 0.419T_{xi} + 0.864T_{mi} - 0.003WD_i - 0.005WS_i$	0.3	
Dunagiri Glacier, Dhauliganga Basin	30°33′-30°35′N 79°52′-79°54′E	1985	$Q_i = 0.681 + 0.774{}^*Q_{i-1} - 0.065{}^*R_{i-2}$	0.7	Srivastava et al. (2014b)
		1987	$Q_i = 0.187 + 0.946{}^*Q_{i-1} - 0.016{}^*R_{i-2}$	0.9	
		1988	$Q_i = 0.146 + 0.967{}^*Q_{i-1} - 0.065{}^*R_i$	0.9	
		1989	$Q_i = 0.332 + 0.832{}^*Q_{i-1} - 0.065{}^*R_{i-2}$	0.7	
		(1985-1989)	$Q_i = 0.172 + 1.144{}^*Q_{i-1} - 0.188{}^* Q_{i-2} - 0.025 {}^*R_i$	0.9	
Gangotri Glacier, Bhagirathi Basin	30°43′-31°01′N 79°0′-79°17′E	2000	$Q_i = 1.593 + 0.911Q_{i-1} + 2.787T_i - 0.789T_{i-1} - 1.611T_{i-2} + 0.487R_i$	0.9	Singh et al. (2010)
		2001	$Q_i = 11.389 + 1.009Q_{i-1} + 0.195T_i - 2.085T_{i-1} - 0.630T_{i-2} + 0.658R_i$	0.9	
		2002	$Q_i = 3.507 + 1.005Q_{i-1} + 2.096T_i - 1.326T_{i-1} - 1.227T_{i-2} + 0.136R_i$	0.9	
		2003	$Q_i = 9.281 + 1.044Q_{i-1} + 1.582T_i - 2.167T_{i-1} - 0.895T_{i-2} + 0.724R_i$	0.9	
		2004	$Q_i = 11.649 + 1.018Q_{i-1} + 0.752T_i - 1.266T_{i-1} - 0.867T_{i-2} + 0.304R_i$	0.9	
		(2000-2004)	$Q_i = 7.649 + 0.995Q_{i-1} + 1.450T_i - 1.523T_{i-1} - 0.710T_{i-2} + 0.227R_i$	0.9	
Dokriani Glacier, Bhagirathi Basin	30°43′-31°01′N 79°0′-79°17′E	1996	$Q_i = -0.827 + 0.918 Q_{i-1} + 0.188 T_i - 0.090 T_{i-1} + 0.007 R_i - 0.018R_{i-1}$	0.9	Singh et al. (2000)
		1997	$Q_i = -0.847 + 0.889Q_i + 0.323 T_i - 0.174 T_{i-1} + 0.029 R_i + 0.004 R_{i-1}$	0.9	
		1998	$Q_i = -1.282 + 0.772 Q_{i-1} + 0.223 T_i + 0.019 T_{i-1} - 0.006 R_i - 0.002 R_{i-1}$	0.7	
		(1996-1998)	$Q_i = -0.671 + 0.901 Q_{i-1} + 0.125 T_i + 0.016R_i$	0.9	
Arctic and other alpine glaciers					
Mikkiglaciaren, Sweden	67°25′N, 17°42′E		$Q_i = 0.329 + 0.546 Q_{i-1} + 0.035T_{mi} + 0.0014NRH_i$	0.8	Stenborg (1970)
Quviagiviaa and Nirukikttuq Glacier, Arctic	79°33.98′N 83°20.48′W		$Q_i = 0.315 T_i + 0.00248 K_i + 0.00021NRH_i + 0.1176W_i$	0.8	Wolfe and English (1995)
Haig Glacier, Alberta, Canada	50°43′N 115°18′W		$Q_i = 0.386 + 0.630 Q_{i-1} + 0.041T_i + 0.0002K_i$	0.9	Shea et al. (2005)

T_{ni} = Minimum temperature, T_{xi} = Maximum temperature, T_{mi} = Mean temperature, WS = Wind speed, R = Rainfall, Q_i = daily mean discharge, Q_{i-1} = discharge lagged by 1 day, T_i = daily mean temperature, T_{i-1} = temperature lagged by 1 day, T_{i-2} = temperature lagged by 2 days, R_i = daily rainfall, H_i=relative humidity, K_i = daily incoming solar radiation, NRH_i= daily net radiation hours, W_i = average daily wind speed. (Discharge in m^3/s, temperature in °C, rainfall in mm, wind speed in m/s, relative humidity in %,vapour pressure in mb, radiation in W/m^2 /*Langley/d).

been done in order to develop multivariate regression models for other Indian Himalayan glaciers and high-Arctic alpine glaciers of the world (Table 10). The current study has been done for only four ablation seasons that may be the reason for lower values of R^2 as compared to other studies.

4. Conclusions

The majority of climate change impact studies are based on observed records confined to lower elevations and they cannot be extrapolated for understanding higher elevation environments. The recent need for generating long term records from higher elevations has brought attention to expand glaciological studies in the Indian Himalayan region. Therefore, based on present investigations the current results can be summarized as follows:

- Four ablation meteorological records show that temperature variations in air temperature are significantly lower, while variations in daily and seasonal rainfall patterns are characterized by heavy rainfall events of ~160 mm/d in the study basin. The

glaciers of the upper Ganga basin (UGB) show varied microclimatic conditions reflecting humid-temperate and semi-arid environment during the ISM season. Relative Humidity is relatively low before the onset and after the withdrawal of the ISM, while the reverse phenomenon is seen for the peak ISM months.

- The SSC follows the discharge patterns showing a rising trend during the onset of ablation and declining trend towards the end of ablation. Quantitative assessment of meltwater discharge and suspended sediments suggest that July and August contributed 66% of melt runoff that transported 76% of the total SSL. Variations in resultant discharge have been observed because of strong storage characteristics and varying meteorological conditions affecting the release of glacier melt. The SSC shows poor correlations with meltwater discharge at a daily scale, while SSL shows significant correlations with meltwater discharge.

- The SSY for central Himalayan glaciers are highest compared to Karakoram and western Himalayan glaciers because of the meteorological influence on discharge affecting sediment transport patterns, hydrological events from the subglacial conduits, topography of the catchment, and lithological variations.

- Flow and load duration curves indicates the flow corresponding to Q_{50}, Q_{75}, and Q_{90} dependability as 4.2, 3.7, and 2.8 m^3/s; and SSL's as 409.0, 266.0, and 157.2 t/d, respectively, for these dependability levels, reflecting the availability of resultant runoff and sediment stored within the glacier conduits. Thus, duration curves should be used for understanding hydrological characteristics over large river basins.
- The regression equations developed for the each ablation season indicate that by including daily meteorological records (rainfall, temperature, and wind velocity) of one station as independent variables, the correlations coefficient varies significantly for each ablation season, which may be caused by the effect of the high variability in rainfall and air temperature during the study period. Therefore, flow forecasting is necessary in the high elevation glacierized basins that highlight such variability in the hydrological database and to improve multiple correlations by installing more automatic weather stations (AWS) within the IHR at different elevations.

Considering various difficulties involved in installing and maintaining hydrometeorological instruments at high elevation sites, the current results suggest that detailed understanding is still required at different climatic zones. Therefore, future studies should follow homogenous time periods that are analogous to other studies during the ablation season over the Indian Himalayan glaciers.

Acknowledgements

References

Allen, S. K., Rastner, P., Arora, M., Huggel, C., & Stoffel, M. (2015). Lake outburst and debris flow disaster at Kedarnath, June 2013: Hydrometeorological triggering and topographic predisposition. *Landslides, 13*(6), 1479–1491.

Andreassen, L. M., van den Broeke, M. R., Giesen, R. H., & Oerlemans, J. (2008). A 5 year record of surface energy and mass balance from the ablation zone of Storbreen, Norway. *Journal of Glaciology, 54*(185), 245–258.

Arora, M., Goel, N., Singh, P., & Singh, R. (2005). Regional flow duration curve for a Himalayan river Chenab. *Hydrology Research, 36*, 193–206.

Arora, M., Kumar, R., Kumar, N., & Malhotra, J. (2014). Assessment of suspended sediment concentration and load from a large Himalayan glacier. *Hydrology Research, 45*(2), 292–306.

Azam, M. F., Ramanathan, A. L., Wagnon, P., Vincent, C., Linda, A., & Pottakal, J. G. (2016). Meteorological conditions, seasonal and annual mass balances of Chhota Shigri Glacier, western Himalaya, India. *Annals of Glaciology, 57*(71), 328–338.

Bhambri, R., Bolch, T., Chaujar, R. K., & Kulshreshtha, S. C. (2011). Glacier changes in the Garhwal Himalaya, India, from 1968 to 2006 based on remote sensing. *Journal of Glaciology, 57*(203), 543–556.

Bhambri, R., Mehta, M., Dobhal, D. P., Gupta, A. K., Pratap, B., Kesarwani, K., & Verma, A. (2016). Devastation in the Kedarnath (Mandakini) Valley, Garhwal Himalaya, during 16–17 June 2013: A remote sensing and ground-based assessment. *Natural Hazards, 80*(3), 1801–1822.

Bhutiyani, M. R. (2000). Sediment load characteristics of a proglacial stream of Siachen Glacier and the erosion rate in Nubra valley in the Karakorum Himalayas, India. *Journal of Hydrology, 227*(1–4), 84–92.

Bollasina, M., Bertolani, L., & Tartari, G. (2002). Meteorological observations at high altitude in the Khumbu valley, Nepal Himalayas, 1994–1999. *Bulletin of Glaciological Research, 19*, 1–11.

Braithwaite, R. J. (2009). Calculation of sensible-heat flux over a melting ice surface using simple climate data and daily measurements of ablation. *Annals of Glaciology, 50*(50), 9–15.

Cánovas, J. B., Trappmann, D., Shekhar, M., Bhattacharyya, A., & Stoffel, M. (2017). Regional flood-frequency reconstruction for Kullu district, western Indian Himalayas. *Journal of Hydrology, 546*, 140–149.

Chen, F., Cai, Q., Sun, L., & Lei, T. (2016). Discharge-sediment processes of the Zhadang Glacier on the Tibetan Plateau measured with a high frequency data acquisition system. *Hydrological Processes, 30*(23), 4330–4338.

Collins, D. N. (1989). Seasonal development of subglacial drainage and suspended sediment delivery to meltwaters beneath an Alpine glacier. *Annals of Glaciology, 13*, 45–50.

Collins, D. N. (1990). Seasonal and annual variations of suspended sediment transport in meltwaters draining from an Alpine glacier. In Hydrology in Mountainous Regions, I, Hydrological Measurements: The Water Cycle. *Proceedings of two Lausanne Symposia IAHS Publication, 193*, 439–446.

Collins, D.N. (1996). Sediment transport from glacierized basins in the Karakoram Mountains. In Erosion and sediment yield: Global and regional perspectives, In: *Proceedings of the Exeter Symposium*, IAHS Publication, 236, 85–96.

Dobhal, D. P., Mehta, M., & Srivastava, D. (2013). Influence of debris cover on terminus retreat and mass changes of Chorabari Glacier, Garhwal region, Central Himalaya, India. *Journal of Glaciology, 59*, 961–971.

Engelhardt, M., Ramanathan, A. L., Eidhammer, T., Kumar, P., Landgren, O., Mandal, A., & Rasmussen, R. (2017). Modelling 60 years of glacier mass balance and runoff for Chhota Shigri Glacier, western Himalaya, Northern India. *Journal of Glaciology, 63*(240), 618–628.

Gao, M., Han, T., Ye, B., & Jiao, K. (2013). Characteristics of melt water discharge in the Glacier No. 1 basin, headwater of Urumqi River. *Journal of Hydrology, 489*, 180–188.

Guerrero, J. L., Westerberg, I. K., Halldin, S., Xu, C. Y., & Lundin, L. C. (2012). Temporal variability in stage–discharge relationships. *Journal of Hydrology, 446*, 90–102.

Hallet, B., Hunter, L., & Bogen, J. (1996). Rates of erosion and sediment evacuation by glaciers: A review of field data and their implications. *Global and Planetary Change, 12*(1), 213–235.

Haritashya, U. K., Kumar, A., & Singh, P. (2010). Particle size characteristics of suspended sediment transported in meltwater from the Gangotri Glacier, central Himalaya—An indicator of subglacial sediment evacuation. *Geomorphology, 122* (1), 140–152.

Haritashya, U. K., Singh, P., Kumar, N., & Gupta, R. P. (2006). Suspended sediment from the Gangotri Glacier: Quantification, variability and associations with discharge and air temperature. *Journal of Hydrology, 321*, 116–130.

Hodgkins, R., Cooper, R., Wadham, J., & Tranter, M. (2003). Suspended sediment fluxes in a high-Arctic glacierised catchment: Implications for fluvial sediment storage. *Sedimentary Geology, 162*(1), 105–117.

Hodgkins, R., Tranter, M., & Dowdeswell, J. A. (1997). Solute provenance, transport and denudation in a high Arctic glacierized catchment. *Hydrological Processes, 11*(14), 1813–1832.

Jansson, P., Hock, R., & Schneider, T. (2003). The concept of glacier storage: A review. *Journal of Hydrology, 282*(1), 116–129.

Kociuba, W. (2017). Determination of the bedload transport rate in a small proglacial high Arctic stream using direct, semi-continuous measurement. *Geomorphology, 287*, 101–115.

Kumar, A. (2011). *Modelling of streamflow and sediment delivery characteristics of Gangotri Glacier basin, Himalayas (Doctoral dissertation)*. Chandigarh, India: Department of Geology, Panjab University.

Kumar, A., Asthana, A. K. L., Priyanka, R. S., Jayangondaperumal, R., Gupta, A. K., & Bhakuni, S. S. (2017). Assessment of landslide hazards induced by extreme rainfall event in Jammu and Kashmir Himalaya, northwest India. *Geomorphology, 284*, 72–87.

Kumar, A., Gokhale, A. A., Shukla, T., & Dobhal, D. P. (2016). Hydroclimatic influence on particle size distribution of suspended sediments evacuated from debris-covered Chorabari Glacier, upper Mandakini catchment, central Himalaya. *Geomorphology, 265*, 45–67.

Kumar, A., Verma, A., Dobhal, D. P., Mehta, M., & Kesarwani, K. (2014). Climatic control on extreme sediment transfer from Dokriani Glacier Garhwal Himalaya. *Journal of Earth System Science, 123*(1), 109–120.

Li, S., Yao, T., Yang, W., Yu, W., & Zhu, M. (2016). Melt season hydrological characteristics of the Parlung No. 4 glacier, in Gangrigabu Mountains, southeast Tibetan Plateau. *Hydrological Processes, 30*, 1171–1196.

Li, Z., Wang, W., Zhang, M., Wang, F., & Li, H. (2010). Observed changes in streamflow at the headwaters of the Urumqi River, eastern Tianshan, central Asia. *Hydrological Processes, 24*, 217–224.

Liu, C., Walling, D. E., & He, Y. (2017). The International Sediment Initiative case studies of sediment problems in river basins and their management. *International Journal of Sediment Research*. (In press)(doi: 1016/j.ijsrc.2017.05.005).

Marquínez, J., Lastra, J., & García, P. (2003). Estimation models for precipitation in mountainous regions: The use of GIS and multivariate analysis. *Journal of Hydrology, 270*(1), 1–11.

Nandy, S.N., Pant, R., & Rao, K.S. (2000). *Indian Himalaya 'a demographic database'*(ENVIS MonographNo. 2). G.B Pant Institute of Himalayan Environment and Development. Almora, ISSN 0972–1819.

Neupane, R. P., Yao, J., & White, J. D. (2014). Estimating the effects of climate change on the intensification of monsoonal-driven stream discharge in a Himalayan watershed. *Hydrological Processes, 28*, 6236–6250.

Orwin, J. F., Lamoureux, S. F., Warburton, J., & Beylich, A. (2010). A framework for characterizing fluvial sediment fluxes from source to sink in cold environments. *Geografiska Annaler, 92*(A), 155–176.

Orwin, J. F., & Smart, C. C. (2004). Short-term spatial and temporal patterns of suspended sediment transfer in proglacial channels, Small River Glacier, Canada. *Hydrological Processes, 18*(9), 1521–1542.

Ostrem, G. C. (1964). A method of measuring discharge in turbulent streams. *Geographical Bulletin, 21*(21), 43.

Pradhananga, N. S., Kayastha, R. B., Bhattarai, B. C., Adhikari, T. R., Pradhan, S. C., Devkota, L. P., Shrestha, A. B., & Mool, P. K. (2014). Estimation of discharge from Langtang River basin, Rasuwa, Nepal, using a glacio-hydrological model. *Annals of Glaciology, 55*(66), 223–230.

Puri, V.M.K. (1999). Glaciohydrological and suspended sediment load studies in the melt water channel of Changme Khangpu Glacier, Mangam district, Sikkim. *Symposium on Snow, Ice and Glaciers – Himalayan Prospective*, Lucknow, 1.

Puri, V. M. K., & Swaroop, S. (1995). Relationship of glacierized area and summer mean daily discharge of glacier basins in Jhelum, Satluj and Alaknanda catchments in North western Himalaya. *Geological Survey of India, Special Publication, 21*(2), 315–319.

Raina, V. K. (2009). *Himalayan glaciers: A state-of-art review of glacial studies, glacial retreat and climate change (MoEFF Discussion Paper)*. G.B. Pant Institute of Himalayan Environment and Development. Kosi-Katarmal, Almora: Ministry of Environment and Forests, Government of India.

Rickenmann, D., Antoniazza, G., Wyss, C. R., Fritschi, B., & Boss, S. (2017). Bedload transport monitoring with acoustic sensors in the Swiss Albula mountain river. *Proc IAHS, 375*, 5–10. http://dx.doi.org/10.5194/piahs-375-5-2017.

Ruiz-Villanueva, V., Allen, S., Arora, M., Goel, N. K., & Stoffel, M. (2017). Recent catastrophic landslide lake outburst floods in the Himalayan Mountain Range. *Progress in Physical Geography, 41*(1), 3–28.

Sangewar, C.V., & Shukla, S.P. (2009). *Inventory of the Himalayan glaciers*. Geological Survey of India, Special Publication No. 34, Kolkata, ISSN 0254–0436.

Shah, S. K., Bhattacharyya, A., & Shekhar, M. (2013). Reconstructing discharge of Beas River basin, Kullu Valley, Western Himalaya, based on tree ring data. *Quaternary International, 286*, 138–147.

Sharp, M., Tranter, M., Brown, G. H., & Skidmore, M. (1995). Rates of chemical denudation and CO_2 drawdown in a glacier-covered alpine catchment. *Geology, 23*(1), 61–64.

Shea, J. M., Anslow, F. S., & Marshall, S. J. (2005). Hydrometeorological relationships on Haig Glacier, Alberta, Canada. *Annals of Glaciology, 40*, 52–60.

Singh, P., Haritashya, U. K., & Kumar, N. (2007). Meteorological study for Gangotri Glacier and its comparison with other high altitude meteorological stations in Central Himalayan region. *Hydrology Research, 38*(1), 59–77.

Singh, P., Haritashya, U. K., Kumar, N., & Singh, Y. (2006). Hydrological characteristics of the Gangotri Glacier, central Himalayas, India. *Journal of Hydrology, 327* (1), 55–67.

Singh, P., Haritashya, U. K., Ramasastri, K. S., & Kumar, N. (2005). Prevailing weather conditions during summer seasons around Gangotri Glacier. *Current Science, 88* (5), 753–760.

Singh, P., Kumar, A., & Kishore, N. (2011). Meltwater storage and delaying characteristics of Gangotri Glacier (Indian Himalayas) during ablation season. *Hydrological Processes, 25*(2), 159–166.

Singh, P., Kumar, A., Kumar, N., & Kishore, N. (2010). Hydro-meteorological correlations and relationships for estimating streamflow for Gangotri Glacier basin in western Himalaya. *International Journal of Water Resources and Environmental Engineering, 2*(3), 60–69.

Singh, P., & Ramasastri, K.S. (1999). Temporal distribution of Dokriani Glacier melt runoff and its relationship with meteorological parameters (Project Completion Report).Roorkee, National Institute Hydrology.

Singh, P., Ramasastri, K. S., Kumar, N., & Arora, M. (2000). Correlations between discharge and meteorological parameters and runoff forecasting from a highly glacierised Himalayan basin. *Hydrological Sciences Journal, 45*(5), 637–652.

Singh, P., Ramasastri, K. S., Kumar, N., & Bhatnagar, N. K. (2003). Suspended sediment transport from the Dokriani Glacier in the Garhwal Himalayas. *Hydrology Research, 34*, 221–244.

Singh, V. B., & Ramanathan, A. L. (2015). Assessment of solute and suspended sediments acquisition processes in the Bara Shigri Glacier meltwater (western Himalaya, India). *Environmental Earth Sciences, 74*(3), 2009–2018.

Singh, V. B., & Ramanathan, A. L. (2017). Characterization of hydrogeochemical processes controlling major ion chemistry of the Batal Glacier meltwater, Chandra basin, Himachal Pradesh, India. *Proceedings of the National Academy of Sciences, India Section A: Physical Sciences, 87*(1), 145–153.

Singh, V. B., Ramanathan, A. L., Mandal, A., & Angchuk, T. (2015). Transportation of suspended sediment from meltwater of the Patsio Glacier, western Himalaya, India. *Proceedings of the National Academy of Sciences, India Section A: Physical Sciences, 85*(1), 169–175.

Singh, V. B., Ramanathan, A. L., & Pottakkal, J. G. (2016). Glacial runoff and transport of suspended sediment from the Chhota Shigri Glacier, western Himalaya, India. *Environmental Earth Sciences, 75*(8), 1–13.

Singh, V. B., Ramanathan, A. L., Pottakkal, J. G., & Kumar, M. (2014). Seasonal variation of the solute and suspended sediment load in Gangotri Glacier meltwater, central Himalaya, India. *Journal of Asian Earth Sciences, 79*, 224–234.

Smahtkin, V. U. (2001). Low flow hydrology: A review. *Journal of Hydrology, 240*, 147–186.

Srivastava, D., Kumar, A., Verma, A., & Swaroop, S. (2014a). Characterization of suspended sediment in meltwater from glaciers of Garhwal Himalaya. *Hydrological Processes, 28*, 969–979.

Srivastava, D., Kumar, A., Verma, A., & Swaroop, S. (2014b). Analysis of climate and meltwater in Dunagiri Glacier of Garhwal Himalaya (India). *Water Resources Management, 28*, 3035–3055.

Stenborg, T. (1970). Delay of run-off from a glacier basin. *Geografiska Annaler Series A Physical Geography, 52A*(1), 1–30.

Sun, M., Yao, X., Li, Z., & Zhang, M. (2015). Hydrological processes of glacier and snow melting and runoff in the Urumqi River source region, eastern Tianshan Mountains, China. *Journal of Geographical Sciences, 25*(2), 149–164.

Suzuki, R., Fujita, K., Ageta, Y., Naito, N., Matsuda, Y., & Karma (2007). Meteorological observations during 2002–2004 in Lunana region, Bhutan Himalaya. *Bulletin of Glaciological Research, 24*, 71–78.

Tartari, G., Verza, G.P., & Bertolami, L. (1998). Meteorological data at the Pyramid Laboratory Observatory, Khumbu Valley, Sagarmatha National Park, Nepal. In: A. Lami & G. Giussani (Eds.), Limnology of high altitude lakes in the Mt Everest Region (Nepal). Mem. Ist. ital. Idrobiol., 57, 23–40.

Vogel, R. M., & Fennessey, N. M. (1994). Flow-duration curves. I: New interpretation and confidence intervals. *Journal of Water Resources Planning and Management, 120*(4), 485–504.

Walling, D. E., & Collins, A. L. (2008). The catchment sediment budget as a management tool. *Environmental Science Policy, 11*(2), 136–143.

Warburton, J. (1990). *Comparison of bed load yield estimates for a glacial meltwater stream. Hydrology in mountainous regions, I, Hydrological measurements: The water cycle, 193*. IAHS Publication.

Wolfe, P. M., & English, M. C. (1995). Hydrometeorological relationships in a glacierised catchment in the Canadian High Arctic. *Hydrological Processes, 9*, 911–921.